

The Spatial and Emission Properties of the Large [O III] Emission Nebula Near M31

ROBERT A. FESEN,¹ STEFAN KIMESWENGER,^{2,3} J. MICHAEL SHULL,⁴ MARCEL DRECHSLER,⁵ XAVIER STROTTNER,⁶ YANN SAINTY,⁷ BRAY FALLS,⁸ CHRISTOPHE VERGNES,⁹ NICOLAS MARTINO,⁹ SEAN WALKER,¹⁰ AND JUSTIN RUPERT¹¹

¹6127 Wilder Lab, Department of Physics and Astronomy, Dartmouth College, Hanover, NH, 03755, USA

²Universität Innsbruck, Institut für Astro- und Teilchenphysik, Technikerstr. 258, 6020 Innsbruck, Austria

³Universidad Católica del Norte, Instituto de Astronomía, Av. Angamos 0610, Antofagasta, Chile

⁴Department of Astrophysical and Planetary Sciences and CASA, University of Colorado, 389-UCB, Boulder, CO 80309, USA

⁵Équipe StDr, Bärenstein, Feldstraße 17, 09471 Bärenstein, Germany

⁶Équipe StDr, Montfrazé, 01370 Saint Etienne Du Bois, France

⁷54000 Nancy, Lorraine, France

⁸Sierra Remote Observatories, 42120 Bald Mountain Road, Auberry, CA, 93602, USA

⁹Various Amateur Observatory Sites, Lorraine, France

¹⁰MDW Sky Survey, New Mexico Skies Observatory, Mayhill, NM, 88339, USA

¹¹MDM Observatory, Kitt Peak National Observatory, 950 N. Cherry Ave., Tucson, AZ 85719, USA

ABSTRACT

Drechler et al. (2023) reported the unexpected discovery of a 1.5° long [O III] emission nebula 1.2° southeast of the M31 nucleus. Here we present additional images of this large emission arc, called SDSA, along with radial velocity and flux measurements from low-dispersion spectra. Independent sets of [O III] images show SDSA to be composed of broad streaks of diffuse emission aligned NE-SW. Deep $H\alpha$ images reveal no strong coincident emission suggesting a high [O III]/ $H\alpha$ ratio. We also find no other [O III] emission nebulosity as bright as SDSA within several degrees of M31 and no filamentary $H\alpha$ emission connected to SDSA. Optical spectra taken along the nebula's northern limb reveal [O III] $\lambda\lambda 4959, 5007$ emissions matching the location and extent seen in our [O III] images. The heliocentric velocity of this [O III] nebulosity is -9.8 ± 6.8 km s⁻¹ with a peak surface brightness of $(4 \pm 2) \times 10^{-18}$ erg s⁻¹ cm⁻² arcsec⁻² (~ 0.55 Rayleigh). We discuss SDSA as a possible unrecognized supernova remnant, a large and unusually nearby planetary nebula, a stellar bow shock nebula, or an interaction of M31's outer halo with Local Group circumgalactic gas. We conclude that galactic origins for SDSA are unlikely and favor instead an extragalactic M31 halo-circumgalactic cloud interaction scenario, despite the nebula's low radial velocity. We then describe new observations that may help resolve the nature and origin of this large nebulosity so close to M31 in the sky.

Keywords: Galaxies: individual (M31) - galaxies: halo - stars: supernova remnant - ISM: intergalactic medium

1. INTRODUCTION

Beginning with Minkowski (1946, 1947, 1948), Shajn & Gaze (1952), Sharpless (1953), Gum (1953, 1955), and Morgan et al. (1955), optical emission line surveys of the sky have been an especially effective means of identifying various types of emission nebulae such as H II regions, planetary nebulae (PNe), supernova remnants (SNRs), stellar wind-blown bubbles, and stellar outflows. The majority of these surveys have concentrated on detecting $H\alpha$ line emission along the Galactic plane. Recent surveys include the Virginia Tech Spectral-line Survey (VTSS; Dennison et al. 1998), the Southern $H\alpha$ Sky Survey Atlas (SHASSA; Gaustad et al. 2001), the Wisconsin $H\alpha$ Mapper (WHAM; Haffner et al. 2003), the

AAO/UKST SuperCOSMOS $H\alpha$ survey (Parker et al. 2005), and the Issac Newton Telescope Photometric $H\alpha$ Survey of the Northern Galactic Plane (IPHAS; Drew et al. 2005)

The first comprehensive optical survey that included other nebular emission lines besides $H\alpha$ was the 1970's photographic survey of the Galactic plane by Parker et al. (1979). This survey, using a small commercial camera lens mounted ahead of a two-stage image intensifier, generated moderately deep images in $H\beta$, [O III] $\lambda 5007$, $H\alpha$ + [N II] $\lambda\lambda 6548, 6583$, and [S II] $\lambda\lambda 6716, 6731$ line emissions. These images quickly led to the discovery of several large PNe, Wolf-Rayet and OB star ring nebulae, and Galactic SNRs (Gull et al. 1977; Kirshner et al. 1978; Gull & Sofia 1979; Blair et al. 1980; Fesen et al.

1981a,b, 1983; Fesen & Gull 1983; Chu 1981; Bruhweiler et al. 1981; Heckathorn et al. 1982a,b).

Like most emission line surveys, the Parker et al. (1979) survey was limited to the Galactic plane. However, with the advent of sensitive large-format CMOS detectors, together with the development of high transmission ($T \sim 95\%$) narrow passband filters (FWHM $\sim 30 \text{ \AA}$), small aperture telescopes are increasingly discovering new Galactic emission line nebulae, both large and small, and not just regions near the Galactic plane. The combination of wide fields of view and large pixel scales ($\geq 2''$) offered by small telescopes has led to the discovery of dozens of new PNe (Kronberger et al. 2014a,b; Le D u et al. 2022), low surface brightness stellar mass loss nebulosities (Kimeswenger et al. 2021), investigations of faint stellar halos of spiral galaxies (Abraham & van Dokkum 2014; Gilhuly et al. 2022), an assortment of large-scale tidal structures around nearby massive galaxies (Martinez-Delgado 2020), and faint Galactic SNR filaments (How et al. 2018; Fesen et al. 2021).

In an unexpected discovery, Drechsler et al. (2023) detected an extremely faint $\simeq 1.5^\circ$ long [O III] emission arc near M31 through the co-addition of hundreds of exposures obtained with small aperture telescopes (see Fig. 1). This emission arc, named the Strottner-Drechsler-Sainty Object (SDSO), had not been reported previously in any deep broadband or $H\alpha$ images of M31, and has no obvious emission counterpart in X-ray, UV, optical, infrared, or continuum radio surveys. Here we describe more fully the instruments and data that led to the discovery of SDSO and the spatial and emission properties of this large [O III] emission nebulosity near M31. We also discuss various Galactic and extragalactic interpretations of this emission arc.

2. OBSERVATIONS

2.1. Optical Imaging

Images of M31 and its surroundings were obtained on 22 nights, beginning in early 2022 August and continuing in early 2022 November using [O III] 5007 \AA , $H\alpha$ + [N II] $\lambda\lambda 6548, 6583$, and RGB continuum filters from several observing sites in France. These images were taken using a Takahashi FSQ106EDX4 telescope and a 6248×4176 pixel ZWO ASI2600MM Pro CMOS camera. While this system provided a field of view (FOV) of $3.48^\circ \times 2.32^\circ$ with a $2.04''$ pixel $^{-1}$ scale, shifts of pointing centers between images generated a slightly larger final FOV. Narrow passband interference filters (FWHM = 30 \AA) from Antlia¹ were used. Total exposure times were 45.7 hr (274×600 s) in [O III], 41 hr in $H\alpha$ + [N II] (246×600 s), and 4 to 5 hr in each of the broadband RGB filters.

A second set of independent images of M31 was obtained from September through November 2022 at

a dark observing site in California² using two different telescope/camera systems. A series of [O III] images totaling 85.5 hr (513×600 s) plus 3.3 hr exposures in RGB filters were obtained using a Takahashi FSQ106mmEDX3 telescope and a 9576×6388 pixel QHY600 CMOS camera yielding a $5.33^\circ \times 3.56^\circ$ FOV. Narrow passband interference $H\alpha$ + [N II] $\lambda\lambda 6548, 6583$ (FWHM = 50 \AA) and [O III] (FWHM = 30 \AA) filters from Astrodon³ with an image scale of $2.0''$ pixel $^{-1}$ were used. Additional [O III] exposures totaling 24.9 hr (299×300 s) using a Takahashi FSQ130mm telescope and a 9576×6388 pixel Moravian C3-61000 CMOS camera were also obtained, using a 30 \AA wide [O III] filter from Chroma⁴.

Much wider FOV [O III] images of M31 and the vicinity around it were obtained from various dark observing sites in France, using a 135mm f/1.8 lens and a ZWO ASI2400MC Pro CMOS detector. This lens + camera system gave a $15.3^\circ \times 10.2$ deg FOV with an image scale of $9.06''$ pixel $^{-1}$. A series of 84×300 s exposures totaling 7.0 hr was obtained.

We also constructed a $9.2^\circ \times 7.9^\circ$ mosaic of $H\alpha$ + [N II] image of M31 and the region around it from images taken as part of the MDW Sky Survey⁵. This survey employs twin Astro-Physics 130 mm refractors, FLI Proline 16803 CCD cameras, and 30 \AA Astrodon $H\alpha$ filters. This imaging system has a FOV of $3.5^\circ \times 3.5^\circ$ with an image scale of $3.17''$ pixel $^{-1}$, with each region imaged for 4 hr (12×1200 s).

Other deep $H\alpha$ images of M31 available in the public domain⁶ and not part of our M31 imaging campaign were also examined. One was obtained by A. Fryhover using a Rokinon 135 mm f/2.8 telescope and ZWO ASI2600mm pro CMOS camera. Exposures totaling 27.7 hr (166×600 s) were obtained at a dark site in northwestern Oklahoma. Another deep $H\alpha$ image was obtained by V. Peris and A. Lozano from 51 hr of exposures taken at Observatorio Astron mico de Aras de los Olmos in Valencia Spain using a Canon EF400mm lens with an Astronon 50 \AA filter and a QHY600L CMOS camera. This system yielded an image scale of $1.98''$ per pixel. Finally, we examined the VTSS $H\alpha$ image of the M31 region (Dennison et al. 1998).

2.2. Optical Spectra

Low-dispersion optical spectra of the brightest regions of the arc were obtained with the MDM 2.4m Hiltner telescope using Ohio State Multi-Object Spectrograph (OSMOS; Martini et al. 2011). Spectra of

² <https://www.sierra-remote.com/>

³ <https://astrodon.com/>

⁴ <https://www.chroma.com>

⁵ <https://www.mdwskysurvey.org>

⁶ <https://apod.nasa.gov/apod/ap221024.html>

<https://www.astrobin.com/b3f77y/?q=M3120H-alpha>

¹ www.Antliafilter.com

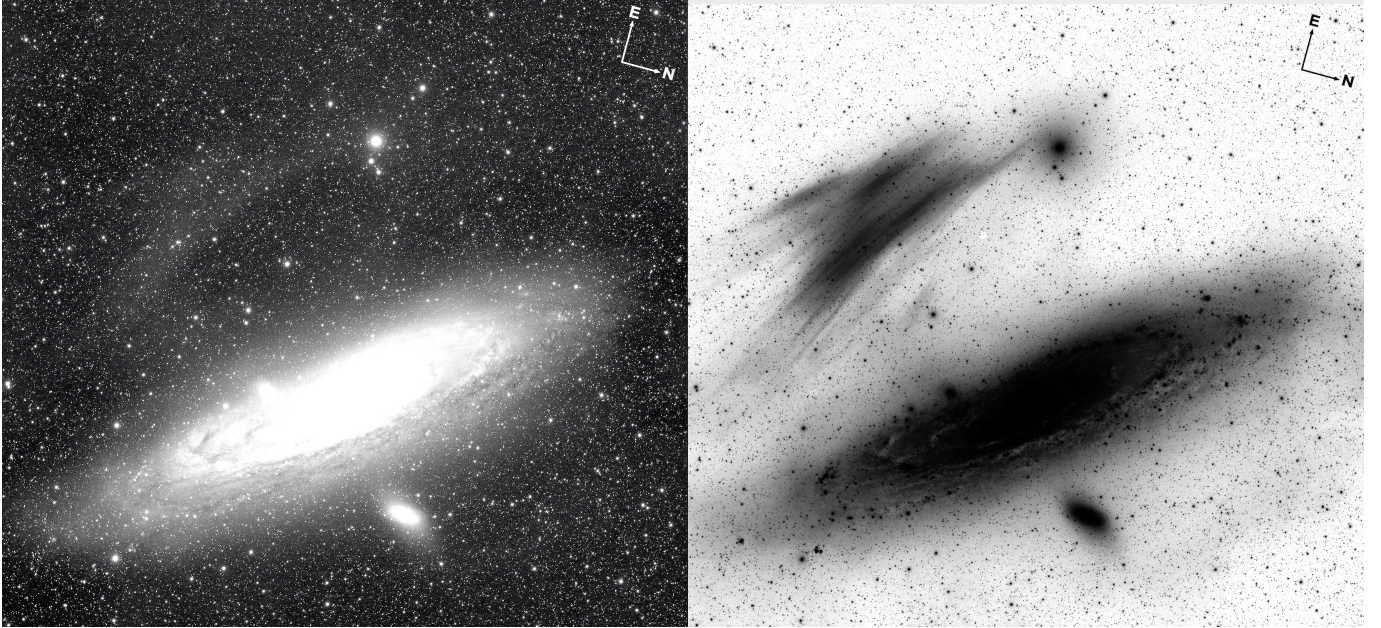


Figure 1. *Left:* Narrow passband 5007 Å image, leading to the discovery of a large, very faint [O III] emission nebula near M31. *Right:* Negative image after blue continuum subtraction and software processing. The bright object near the top center is the 4.5 mag B5 V star HD 4727 (ν Andromeda).

SDSO were taken on 13 January 2023 UT (Slit 1) and again on 25 January 2023 UT (Slit 2). With a VPH grism ($R \simeq 1600$) and a $3.0''$ wide north-south aligned slit, single exposures of 3600 s each were taken at the two slit positions near the arc’s north central edge (Slit 1: RA(J2000) = 00:45:55.9; Slit 2: RA(J2000) = 00:45:39.8). The slit’s effective $16'$ length allowed us to sample both the arc and the largely empty region to the north (see Section 3.5 for further slit position details). While the nominal wavelength coverage for these spectra was 3400–5900 Å, the camera/grism system was most sensitive in the 4000–5000 Å region. For Slit 1, the spectra were binned along the slit ($0.55''$ pixel $^{-1}$). For Slit 2, we employed a 2×2 binning mode, with a dispersion scale 1.45 Å pixel $^{-1}$ and a FWHM resolution of 3.5 Å.

Additional spectra were taken at neighboring locations well off the arc for comparison purposes. For Slit 1, a 3600 s exposure was taken 0.65° to the southeast (J2000; RA = 00:48:32.85, Dec = +39:52:45) where no [O III] is seen in our images. For Slit 2, a 3600 s exposure was taken immediately following the on-target exposure of a blank sky region (J2000; RA = 02:34:09.4, Dec = +40:19:45) with similar hour angle and airmass values to those of the on-target spectrum. For both slits, spectra were extracted after subtraction of off-arc spectra. Wavelength calibrations were made through Hg-Ne, Xe, and Ar comparison lamp spectra along with night sky lines. Data reductions were made using standard IRAF and MIDAS software routines.

2.3. GALEX UV Images

We constructed wide-field GALEX UV images of the [O III] emission region near M31 to investigate possible UV emission like that seen in the filamentary shocks of Galactic SNRs (Fesen et al. 2021). GALEX was a NASA science mission led by the California Institute of Technology, with a 50-cm diameter modified Ritchey-Chrétien telescope, a dichroic beam splitter and astigmatism corrector, and two microchannel plate detectors to simultaneously cover two wavelength bands with a 1.25° field of view with a resolution of $1.5''$ pixel $^{-1}$.

Images were obtained in two broad bandpasses: a far-UV (FUV) channel sensitive to light in the 1344 Å to 1786 Å range and a near-UV (NUV) channel covering 1771 Å to 2831 Å (Morrissey et al. 2007). The resulting images were circular with a FWHM resolution of $\sim 4.2''$ and $\sim 5.3''$ in the FUV and NUV bands, respectively.

3. RESULTS

Figure 1 shows the original sum of 45.7 hr of [O III] images, revealing an emission nebula near M31 discovered by Drechsler et al. (2023) and hereafter referred to as either SDSO or simply as the M31 [O III] arc. The left panel shows the faintness of the arc, even using a narrow passband 30 Å filter and illustrates why the arc was missed in wide band images. Subtraction of background blue and green continuum images makes the nebula obvious, as seen in the negative version in the righthand panel.

The arc’s small-scale details and coordinates can be seen in the enlarged Figure 2. Estimated to be $\simeq 1.5^\circ$

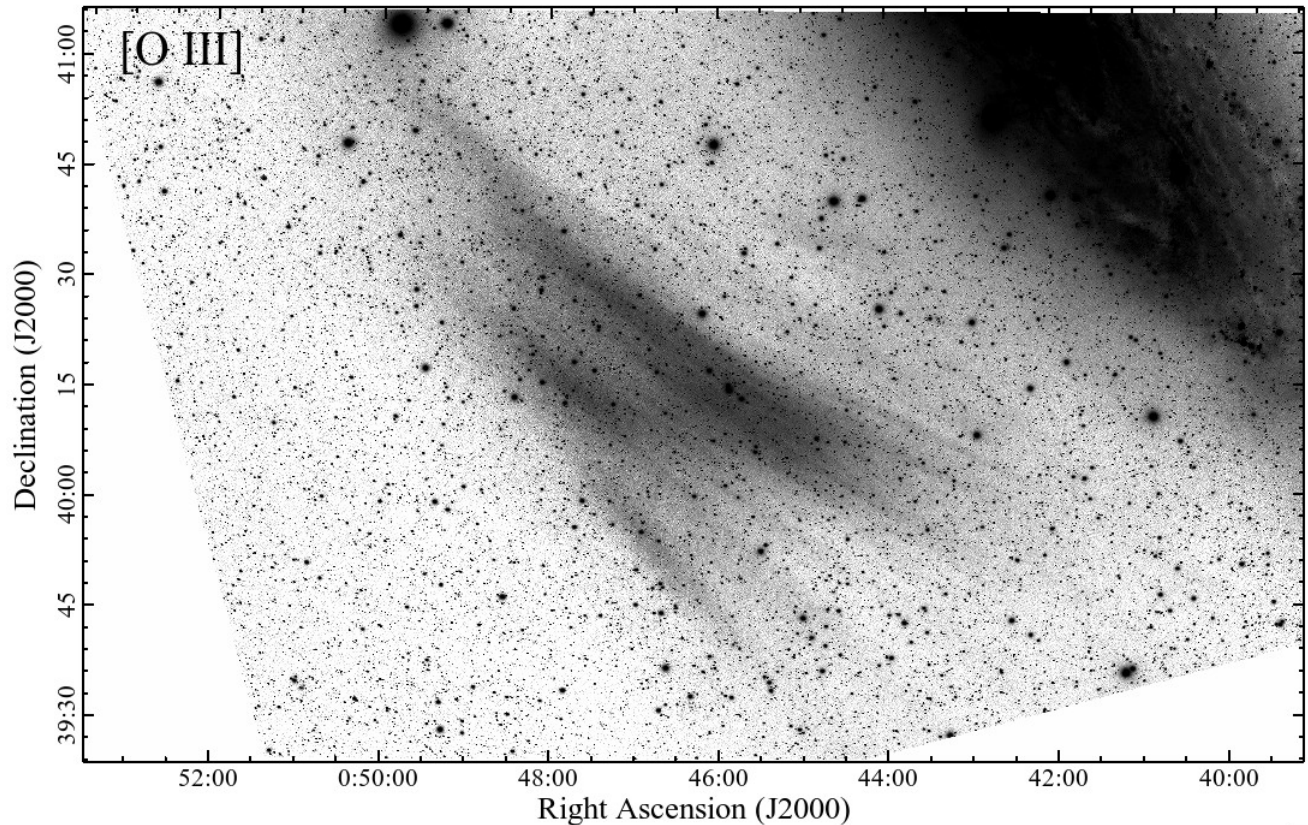


Figure 2. Close-up of the 1.5° long [O III] 5007 Å emission nebula (SDSO) located southeast of M31’s nucleus.

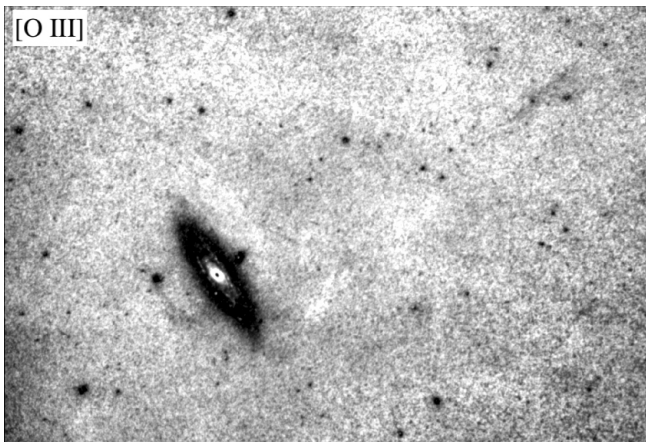


Figure 3. Deep [O III] image of the sky around M31. The FOV as shown is $9.2^\circ \times 14.5^\circ$. North is up, East to the left.

in length, $\simeq 0.5^\circ$ in width and centered some 1.2° southeast of M31’s nucleus (Drechsler et al. 2023), this line-emission nebula appears composed of several broad and gently curved filaments aligned approximately NE-SW. Although displaying a filamentary appearance, the nebula’s overall structure is mainly diffuse. No thin or sharp filaments are visible, as often seen in [O III] SNR filaments and in some PNe.

The nebula is composed of three main and largely aligned emission regions. The nebula’s brightest region lies closest to M31 and extends farthest to both the northeast and southwest. In Figure 2, none of the emission regions exhibit well-defined ends, but instead gradually fade at their NE and SW ends. While the nebula is fairly well defined along its eastern portions, along its western edges, fainter emission bands and patches can be seen lying in between it and M31’s disk.

3.1. No Other [O III] Emission Nebulae Near M31

Drechsler et al. (2023) presented [O III] images of M31’s eastern region, extending 2° from the M31 nucleus and to the west past NGC 205. These data revealed no [O III] emission nebulae around M31 other than SDSO. To investigate this further, we obtained wider FOV [O III] images. These indicate that, with the exception of an emission cloud 8° northwest of M31, SDSO appears to be an isolated [O III] nebula located relatively close in projection to M31.

This can be seen in Figure 3, where we present a $9.2^\circ \times 14.5^\circ$ [O III] image of M31 and its surroundings. The curvature of SDSO and the lack of any detected [O III] emission outside of M31’s disk on the opposite side of M31 from SDSO suggest that this is an isolated emission feature and not part of a larger [O III] emission structure. Because this image is the result of

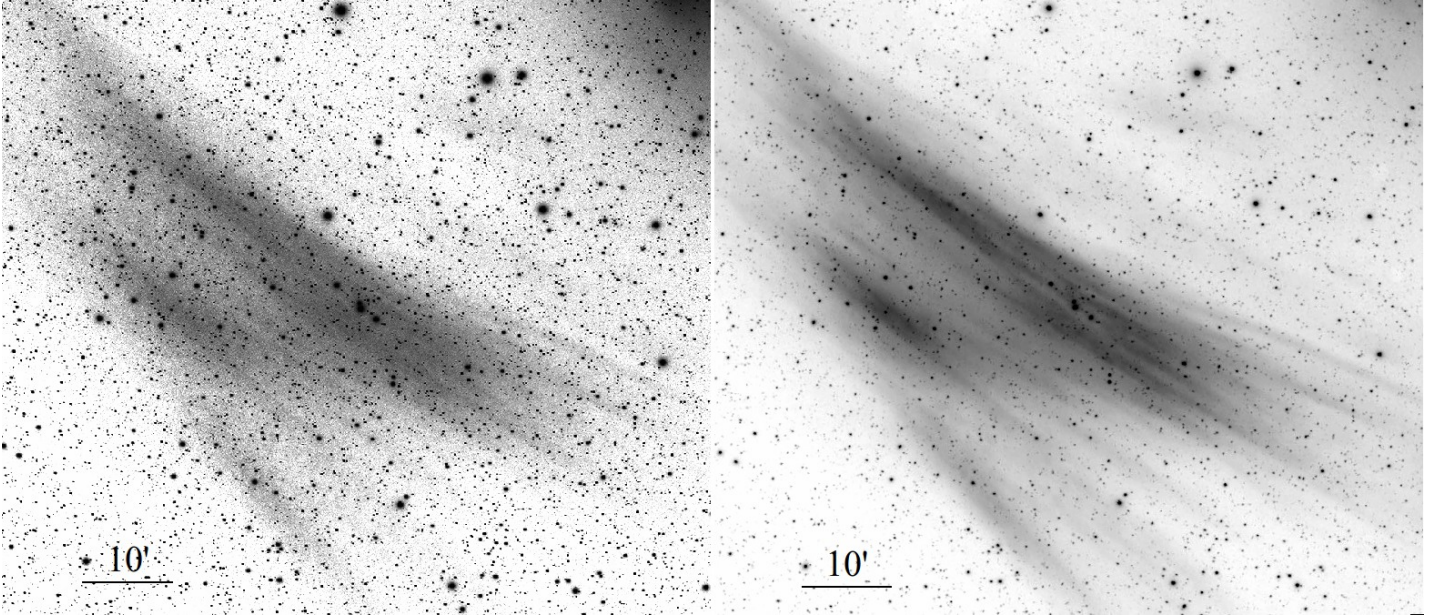


Figure 4. Spatial emission details of SDSO as seen in two independent sets of deep [O III] 5007 Å images. Exposure totals were 46 hr and 110 hr for the left and right images, respectively. North is up, East to the left.

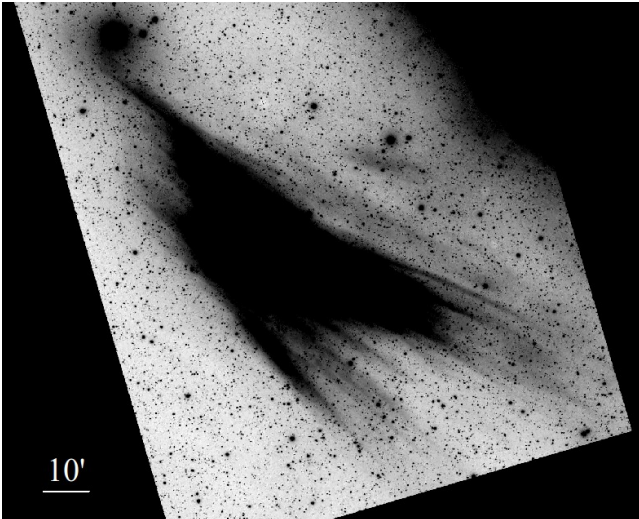


Figure 5. High contrast [O III] image showing SDSO’s maximum extent. North is up, East to the left.

only 7 hr of exposure, SDSO is more poorly detected in this image compared to our other, deeper images. Consequently, we cannot rule out the presence of other extended [O III] nebulae around M31 with a surface brightness much lower than that of SDSO. Nonetheless, it is clear that no similarly bright [O III] emission feature lies within several degrees of M31.

3.2. SDSO’s Substructure and Extent

An independent and slightly deeper [O III] image set confirms and clarifies the nebula’s fine-scale structure. This is shown in Figure 4, where the left panel shows

the discovery [O III] image made from 45.7 hr of exposures (Drechsler et al. 2023), with the right panel image composed of a separate set of 110 hr of [O III] exposures. Both images as shown are the products of significant post-processing using various commercial image software. However, the fact that nearly identical arc substructures are seen in the two images obtained using different telescope + camera systems supports the reality of SDSO’s substructures as seen in these images.

We note that since the images were taken over a long period of time spanning months, telluric airglow emissions and other night sky contamination can be ruled out. Small scale structures change on timescales of minutes and at most hours (Noll et al. 2012; Jones et al. 2019) and only add a constant background. Seasonal variations of the background causing long time-scale biannual fluctuations are well studied (Noll et al. 2017) and can also be ruled out. Finally, post processing was done on individual images near in time blocks before co-adding with all image subgroups show the same morphology.

The longer exposure image (Fig. 4, right panel) shows SDSO to be entirely diffuse in structure, with its filamentary appearance mainly due to several long and broad streaks of diffuse emission rather than thin, sharp filaments. This longer exposure image also shows that SDSO’s emission extends farther to the SW and off the image frame shown.

The full extent of SDSO’s emission can be seen in the higher contrast version presented in Figure 5. This shows that the nebula’s maximum NE-SW length is larger than the 1.5° estimated by Drechsler et al. (2023) and is closer to 2°, extending from its NE tip near the

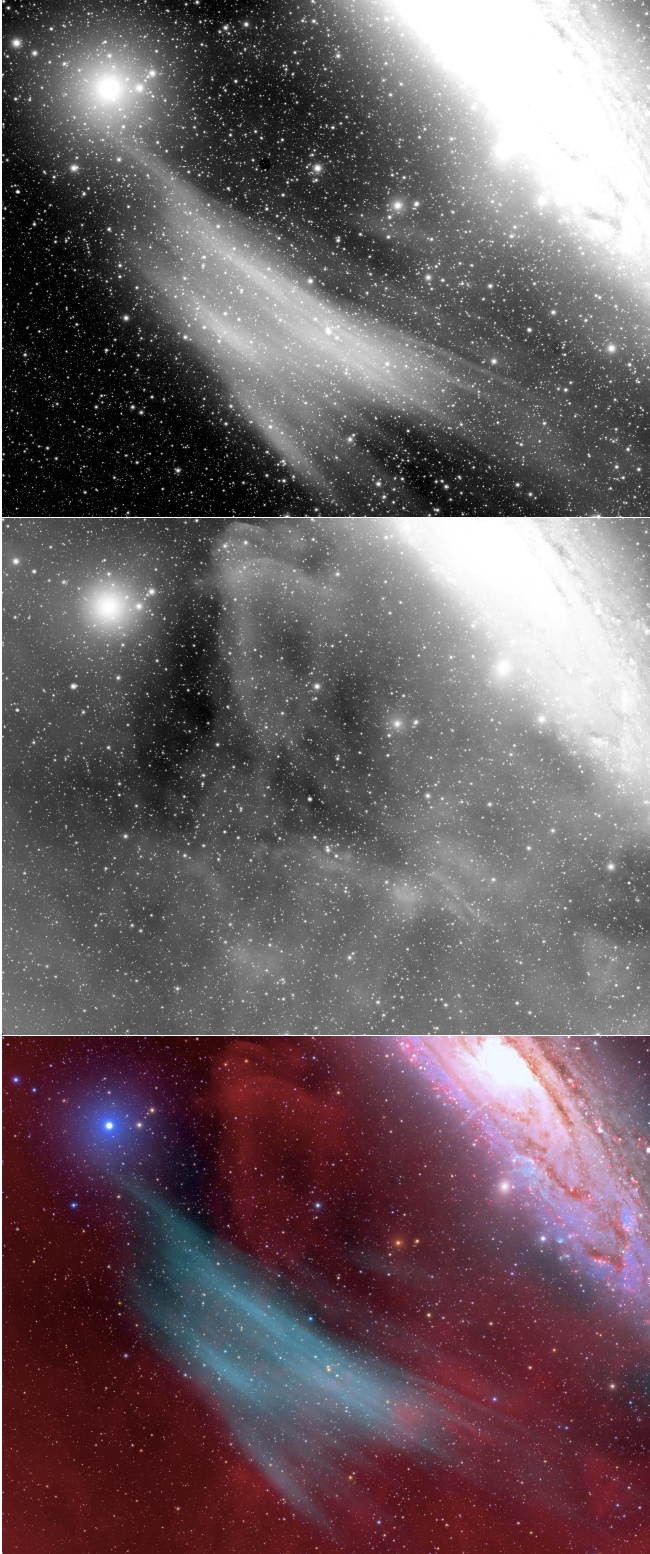


Figure 6. Matching [O III] (top) and $H\alpha + [N II]$ (middle) images along with color composite (bottom) of SDSSO and its immediate surroundings. North is up, East to the left.

B5 V star HD 4727 (ν And) down to the far right-hand

corner (RA = 00:41, Dec = +39:45) where the emission fans out into two broad diffuse branches. Lastly, this higher contrast image also highlights the arc’s nearly straight eastern edge. Interestingly, this eastern edge exhibits a position angle (PA) of $\simeq 40^\circ$ which is nearly the same as the PA of 38° for M31’s major axis (de Vaucouleurs 1958; Walterbos & Kennicutt 1987).

3.3. Projected $H\alpha$ Emission Nebulae Near M31

Drechsler et al. (2023) reported finding no bright $H\alpha$ emission nebulae coincident with the SDSSO nebula and estimated a ratio $I([O III]\lambda\lambda 4959, 5007)/I(H\alpha) \geq 5$ for the nebula’s brightest regions based on deep but uncalibrated [O III] and $H\alpha$ images. Below we discuss deep $H\alpha$ images near M31, obtained both by ourselves and others, which indicate no strong coincident $H\alpha$ emission at SDSSO’s location.

Figure 6 shows positive [O III] and $H\alpha + [N II]$ images along with a color composite of these images. This figure shows that there is little $H\alpha$ emission coincident with the [O III] arc. The detected $H\alpha$ emission displays a very different morphology to that seen in the [O III] image suggesting no association with the arc. This is highlighted in the color image which suggests a high [O III]/ $H\alpha$ ratio for a majority of the arc.

Figure 7 presents wider FOV $H\alpha + [N II]$ images of M31 and its immediate neighborhood obtained with a variety of instruments and exposures⁷. The top right panel image was obtained by us, and the top left was obtained by A. Fryhover. (Note: A nearly identical $H\alpha$ image to Fryhover’s image was obtained by V. Peris and A. Lozano⁸.) The bottom panel shows a much wider FOV image taken as part of the Virginia Tech Spectral-line Survey (VTSS).

These $H\alpha$ images and those shown in Figure 7 look remarkably similar, despite the range of $H\alpha$ filter widths used; namely, 50 \AA for the top right image, 30 \AA for the top left image, and 17.5 \AA for the VTSS image (bottom panel). Since SDSSO was detected using a 30 \AA wide [O III] $\lambda 5007$ filter, the lack of correlated $H\alpha$ emission with SDSSO does not appear to arise from radial velocity differences between emitted [O III] and $H\alpha$ line emissions.

Most of the detected diffuse $H\alpha$ emission seen here is likely Galactic emission unrelated to M31 with the exception of extended diffuse emission from M31’s warped disk immediately north and south of M31’s bright main disk. Outside of the different FOVs and image resolu-

⁷ Note: The top images labeled “ $H\alpha$ ” were taken with filters also sensitive to the usually much weaker [N II] $\lambda\lambda 6548, 6583$ emission lines. The bottom VTSS image was taken using a 17.5 \AA wide filter that avoided most [N II] emission contamination.

⁸ <https://www.astrobin.com/b3f77y/>

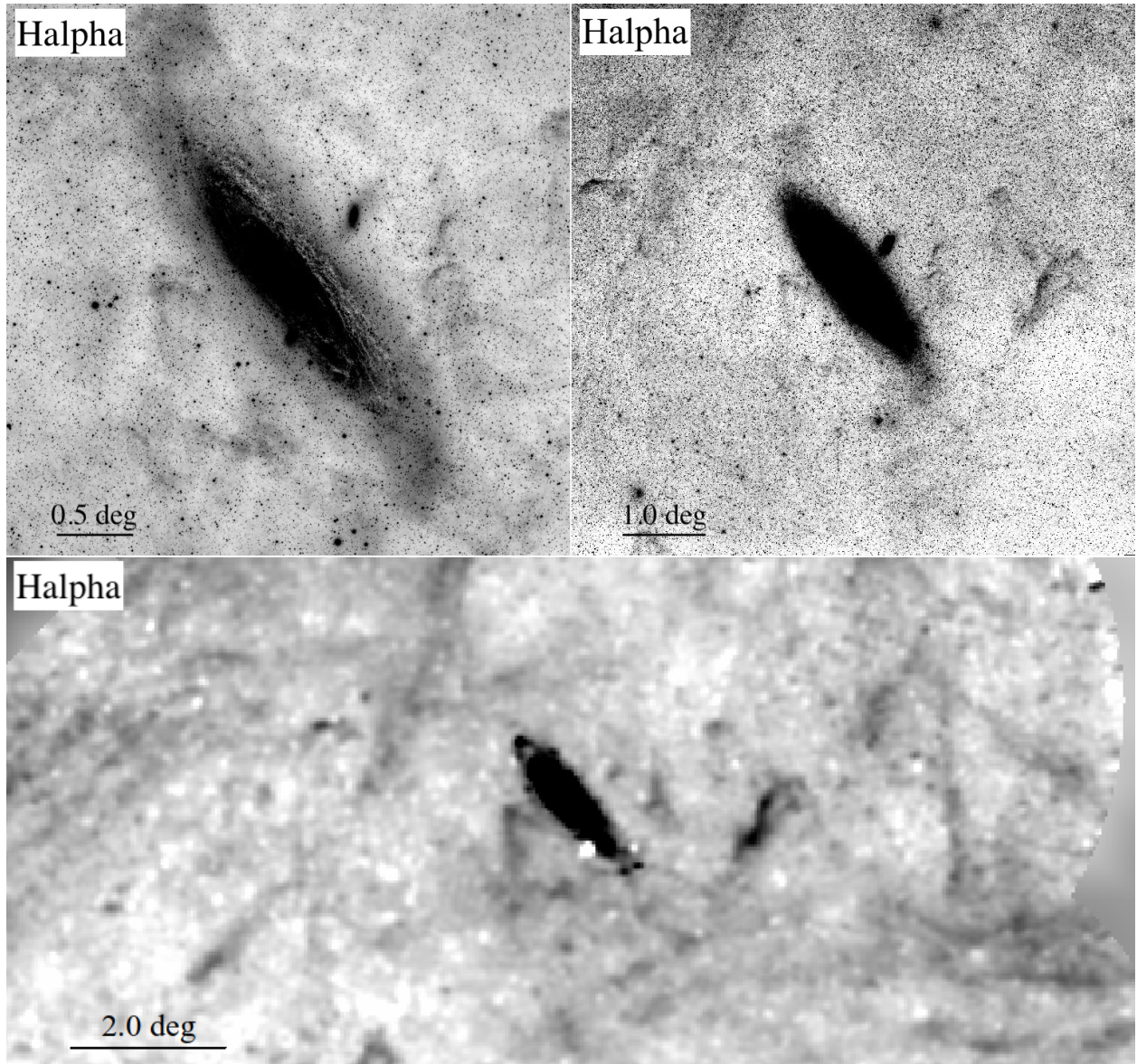


Figure 7. Wide field $H\alpha$ images showing faint emission around M31. Image FOVs as shown are: $3.8^\circ \times 3.8^\circ$ (top left) and $7.1^\circ \times 7.1^\circ$ (top right). Bottom: VTSS $H\alpha$ image; $15.6^\circ \times 7.1^\circ$. North is up, East to the left for all panels.

tions, we find no significant differences in the detected emission features among these $H\alpha$ images. Most importantly, no significant $H\alpha$ emission is seen in the location of SDSO, and none show a similar structure or extent.

3.4. GALEX Images of M31 and the SDSO Region

Nebulae exhibiting bright [O III] emissions are sometimes accompanied by significant far UV line emissions, such as seen in SNRs (Kim et al. 2014; Tutone et al. 2021; Fesen et al. 2021). Because of SDSO’s strong [O III] emission, we have examined GALEX FUV images of M31 to see if SDSO also exhibits detectable FUV emission. A mosaic of GALEX FUV images of M31 and its surroundings is shown in Figure 8. Although wide field GALEX images of M31 have been presented before

(Thilker et al. 2005b), most subsequent UV studies concentrated on M31 point sources and star clusters Kang et al. (2009, 2012); Bianchi et al. (2014); Leahy et al. (2021). None of these papers commented on extended emission outside of the M31 disk.

Figure 8 shows no obvious correlated FUV emission at SDSO’s location. However, given the extreme faintness of SDSO in [O III], it is not clear that a lack of FUV emission seen by GALEX is especially meaningful. We do find considerable diffuse and filamentary nebulousity, seeming to extend radially outward from M31’s southern disk, partially coincident with M31’s Giant Stellar Stream of stars (GSS; Ibata et al. 2001; McConnachie et al. 2003, 2005; van der Marel et al. 2012; Gilbert et al. 2007, 2019; Fardal et al. 2007, 2012). To our knowledge,

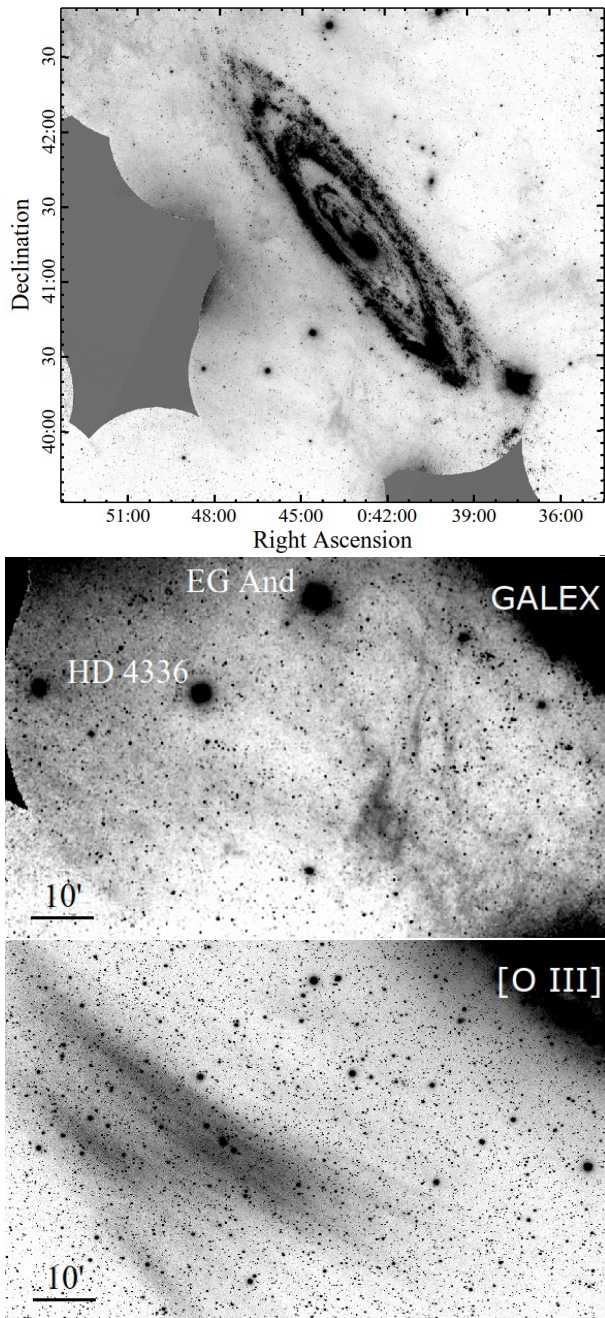


Figure 8. Top Panel: Mosaic of GALEX Far-UV (FUV) images of the M31 and its surroundings. Middle and Bottom Panels: Matching GALEX FUV (middle) and [O III] (bottom) images of the SDO region. The UV bright stars EG And and HD 4336 are marked in the GALEX image.

the presence of far UV filaments at the location of M31’s GSS has not been previously reported despite wide FOV mosaic GALEX FUV images covering this region having been published (Thilker et al. 2005b; Madore 2005).

3.5. Optical Spectra

Low-dispersion optical spectra were obtained at two locations near the northern limb of SDO. The slit positions, labeled Slits 1 and 2, are shown in the middle panel of Figure 9. The slits are 16’ in length and cover a portion of SDO as well as an [O III] emission-free region to the north.

The resulting long-slit 2D spectra obtained at both slit positions are shown in adjacent panels of Figure 9. These show a clear detection of [O III] emission in both slit spectra corresponding to the location of SDO. Its disappearance along the slits is marked by the horizontal dashed lines at the upper edge of the detected emission, as seen in the [O III] image. In the brightest regions, faint emission from both [O III] $\lambda\lambda 4959, 5007$ lines can be seen. Unlike the detected [O III] line emissions, several night sky lines, marked by arrows at the bottom, are seen to be continuous along the full length of the slits.

The outermost panels in Figure 9 show the detected flux for the [O III] $\lambda 5007$ line. The flux drops sharply at the northern edge of SDO, matching our [O III] image. No [O III] line emission was detected with identical exposure times in a region 40’ to the SE from SDO. Because [O III] emission is seen in both Slits 1 and 2 and fades from south to north along the slit, we are confident that we have detected [O III] line emission principally from SDO.

Using night-sky telluric emission lines as zero-point calibrators, notably the [N I] doublet lines at 5197.90 Å and 5200.26 Å, we find heliocentric velocities of -9.8 ± 6.8 km s $^{-1}$ for the [O III] emission lines and $+34 \pm 14$ km s $^{-1}$ for the brighter portion of the detected H β emission seen in the spectrum taken at Slit 2. The individual [O III] velocity measurements taken at 10’’ increments along Slit 2 are shown in Figure 10, along with the blue line representing the average velocity for the H β line.

Figure 11 shows the integrated spectrum for Slit 2 with the wavelengths in the observed telluric rest frame. The displayed Gaussian fit for the [O III] $\lambda 4959$ line used the [O III] $\lambda 5007$ line scaled down 1:3 and shifted to the same radial velocity of -9.8 km s $^{-1}$ of the [O III] $\lambda 5007$ line. The H β fit results in a wider line with a radial velocity of $+34$ km s $^{-1}$. Our velocity results indicate that the H β emission seen along part of Slit 2’s spectrum is not related to SDO’s [O III] emission. This is consistent with our images, which show little H α at SDO.

The surface brightness of SDO’s brighter regions estimated from the data ranges from $(2.5 \pm 2) \times 10^{-18}$ erg s $^{-1}$ cm $^{-2}$ arcsec $^{-2}$ for Slit 1, to $(4 \pm 2) \times 10^{-18}$ erg s $^{-1}$ cm $^{-2}$ arcsec $^{-2}$ for Slit 2. These values are consistent with our earlier estimate reported in Drechsler et al. (2023). These values drop sharply to under 1×10^{-18} erg s $^{-1}$ cm $^{-2}$ arcsec $^{-2}$ at SDO’s northern edge in this region. Using the conversion of 1 Rayleigh = 7.42×10^{-18} erg s $^{-1}$ cm $^{-2}$ arcsec $^{-2}$ for [O III] $\lambda 5007$, we find that SDO’s brighter regions have a surface brightness in [O III] of

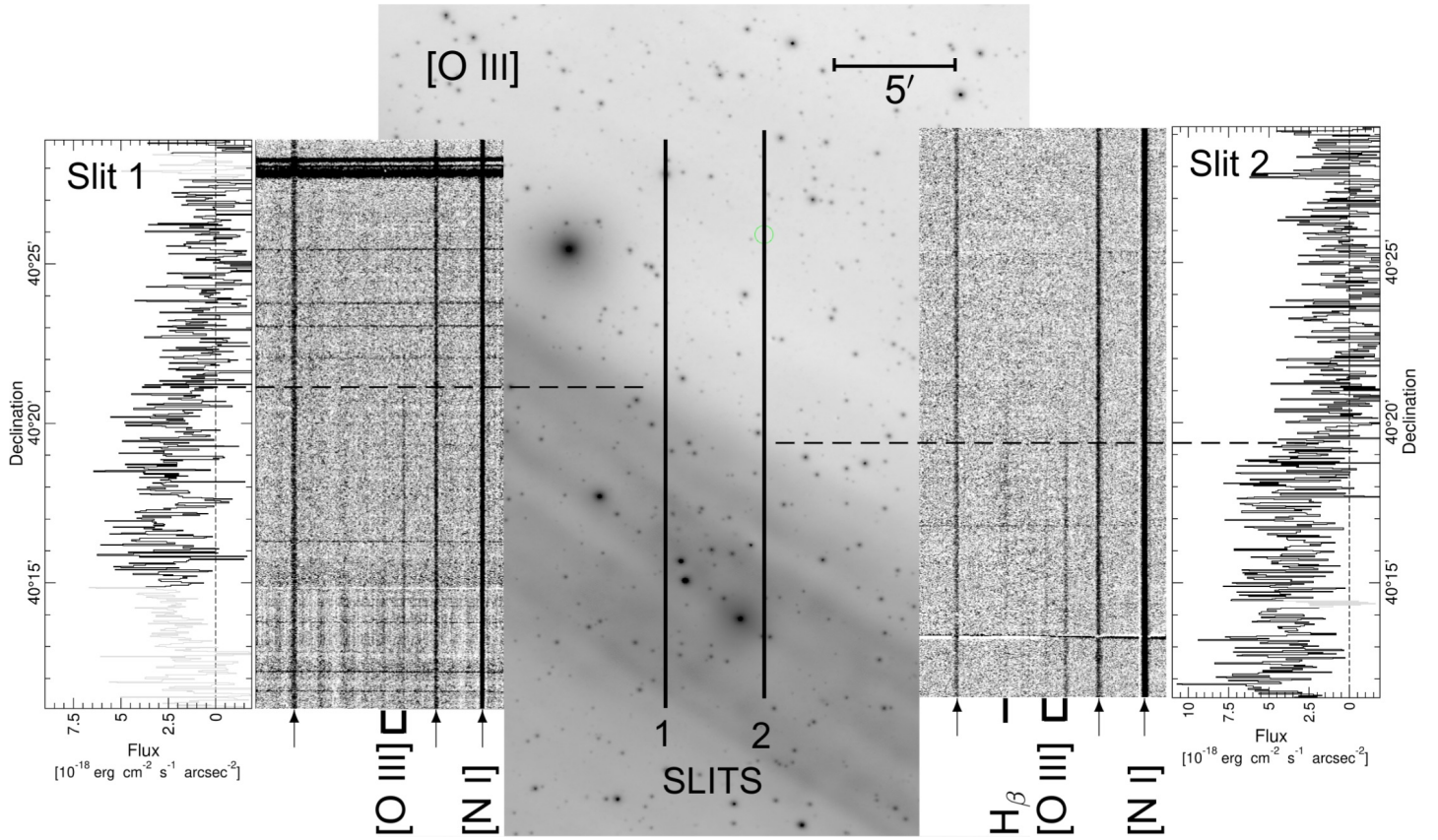


Figure 9. SDO Spectra: The middle panel shows our [O III] $\lambda 5007$ image of SDO with the locations of Slits 1 and 2 indicated. Adjacent left and right panels present resulting 2D spectra and the presence of [O III] $\lambda\lambda 4959, 5007$ emission, which disappears, marked by dashed lines in the clear area north of SDO. Night sky line emissions running the full length of the slits, including [N I] $\lambda\lambda 5198, 5200$, are marked by arrows at the bottom. The two outer panels show plots of the detected [O III] $\lambda 5007$ flux running from south to north along the lengths of both slits.

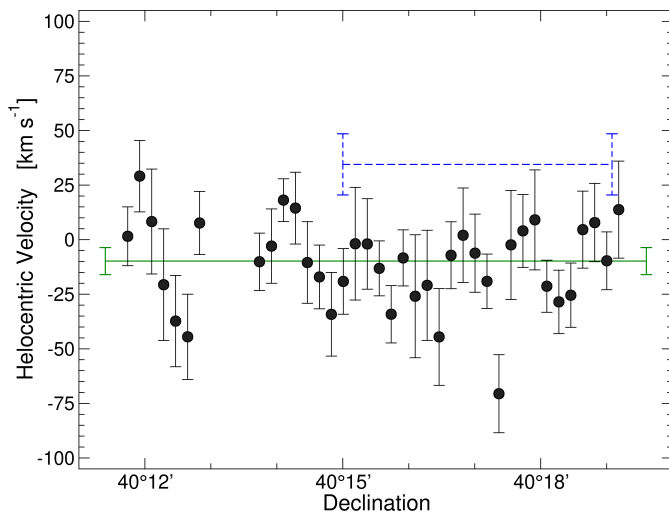


Figure 10. Plot of heliocentric velocities for [O III] $\lambda 5007$ (green line) and H β (dashed blue line) along the Slit 2 moving from south to north. The error bars indicate the statistical errors for the global fit solution, $-9.8 \pm 6.8 \text{ km s}^{-1}$.

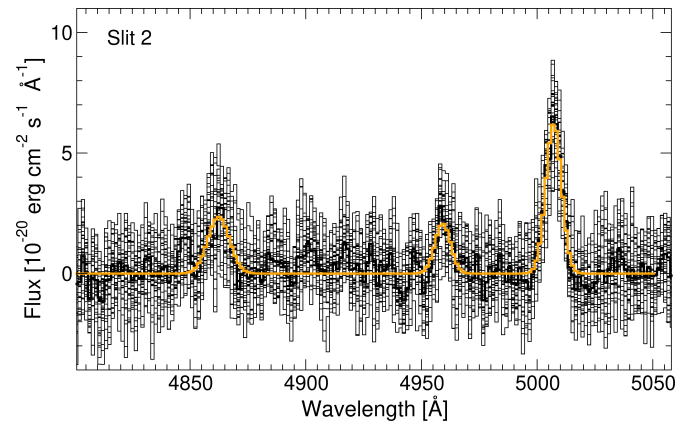


Figure 11. Spectra obtained in Slit 2 around H β and [O III] integrated in $10''$ bins in the region of SDO between $+40^\circ 11' 25'' < \delta < +40^\circ 19' 10''$ (gray lines) and the total averaged spectrum (orange line). The wavelengths shown are in the observed telluric rest frame. The [O III] $\lambda 4959$ line fit used that measured for the [O III] $\lambda 5007$ line.

~ 0.55 Rayleigh, and the faintest regions are detected at ~ 0.2 Rayleigh.

We note that our estimated SDO's [O III] flux and velocity are noticeably different from those reported by Amram et al. (2023) who also obtained spectra of SDO in January 2023 but at a lower resolution than our data. They cite an [O III] velocity of -96 ± 4 km s $^{-1}$, although their listed accuracy seems inconsistent with the resolving power $R \approx 750$ (400 km s $^{-1}$) of their low-resolution spectrograph. They also report detecting strong H α and [N II] emissions and an [O III] surface brightness seven times brighter than our estimate. They cite a surface brightness value of $(2.7 \pm 1.4) \times 10^{-17}$ erg s $^{-1}$ cm $^{-2}$ arcsec $^{-2}$ (3.7 Rayleigh for [O III] $\lambda 5007$).

The source of the discrepancy between their and our measurements is not obvious. It may simply be that their slit sampled a spot a few arc minutes south of our two slit positions where there is a bright diffuse clump of H α emission (see our Fig. 6). This could explain their strong H α and [N II] emissions. However, whereas our 2D spectra clearly show detected [O III] from SDO, [O III] emission is not visible in their 2D background subtracted spectra (their Fig. A.1). In addition, they found H α emission to be roughly twice as bright than [O III] (i.e., H α /[O III] 5007 = 1.5 - 2.8), whereas our images of SDO show no strong or correlated H α emission (see Fig. 6).

4. DISCUSSION

The morphology and emission properties of SDO do not lead us, by themselves, to a definite conclusion about its location and physical nature. The fact that it is presently only detected in optical [O III] line emission, together with the lack of a constraint on its distance and hence its physical size, severely limits our ability to determine its likely nature.

The goal of our spectra of the emission arc was to provide radial velocity information which might establish (or not) an association with M31 and its halo. The Local Group, with M31 and the Milky Way as its two main components, is a bound system decoupled from the Hubble expansion. M31's heliocentric velocity is -300 ± 4 km s $^{-1}$ (Slipher 1913; de Vaucouleurs et al. 1991; McConnachie et al. 2005) of which ~ 200 km s $^{-1}$ is due to the directional component of the Sun's velocity around the Galaxy's center. This leaves the M31 barycenter with an approaching velocity to the Milky Way barycenter of ~ 110 km s $^{-1}$.

Our estimated heliocentric radial velocity for SDO of roughly -10 km s $^{-1}$ would seem, on its face, to strongly favor a Galactic origin, rather than one associated with M31. However, for reasons discussed below, we view a Galactic origin as less likely than an extragalactic origin associated with M31. Below we briefly discuss various possibilities as to the nature of SDO, divided into Galactic and M31 scenarios. We pose three Galactic possibilities: an undiscovered SNR at an unusually high

Galactic latitude, a faint and unusually nearby planetary nebula, or a stellar bow shock nebula. We then discuss the possibility that SDO is an extragalactic nebula possibly related to M31 and offer explanations for its small heliocentric radial velocity.

4.1. A Galactic Origin

4.1.1. A Faint, Undiscovered Galactic SNR

A large and curved nebula displaying strong [O III] emission relative to that of H α might indicate the presence of a faint and previously unknown SNR with a location that just happens to be near M31 by chance. Indeed, based on low-dispersion optical spectra, Amram et al. (2023) tentatively proposed that SDO is the most visible part of a large 35-pc diameter SNR projected near M31 located some 0.7 kpc away. That would correspond to a 0.05-radian (2.86 $^\circ$) angular diameter, placing the far side of the remnant $\sim 1.7^\circ$ northwest of the M31 nucleus, where no emission is apparent (see Figs. 3 and 7).

At a Galactic latitude $b = -22.5^\circ$, a very low surface brightness supernova remnant located near M31 in the sky might have escaped notice in Galactic SNR radio surveys, which have concentrated on regions within $\approx 5^\circ$ of the Galactic plane (e.g., Reich et al. 1990; Duncan et al. 1995; Langston et al. 2000). SDO might also be one of those SNRs where some portion of their optical structure is dominated by [O III] line emission.

The most cited case for this situation is that of the $5.2^\circ \times 4.0^\circ$ remnant G65.3+5.7 located nearly six degrees above the Galactic plane (Gull et al. 1977). This remnant was only discovered due to its strong [O III] emission in the Parker et al. (1979) survey. Nearly all of this remnant's optical emission structure consists of high I($\lambda 5007$)/I(H α) ratios with values as large as $\simeq 10$ (Fesen et al. 1985; Mavromataki et al. 2002; Boumis et al. 2004). While such line ratios are unusual, some remnants display strong [O III] emission over small portions of their optical structure. These include the Cygnus Loop (Fesen & Hurford 1996), CTB 1 (Hailey & Craig 1994; Fesen et al. 1997), and G179.0+2.6 (How et al. 2018).

If SDO were part of an undiscovered SNR, its slight curvature would suggest a fairly large remnant spanning many degrees in angular size. Judging by the arc's most strongly curved inner feature, we estimate a radius $\sim 2^\circ$ assuming a perfectly circular structure. A Galactic remnant this size would be unusual but hardly extraordinary, and its center would lie to the northwest of the M31 center. A SNR located some 22 degrees off the Galactic plane would not likely have a vertical distance more than $z \sim 1.5$ kpc. Consequently, an angular diameter of 4° would imply physical dimensions of 35–105 pc if located 0.5–1.5 kpc distant. These dimensions are typical for a middle-aged or an old SNR. SDO's strong [O III] emission relative to H α would suggest a

shock velocity $\simeq 90 - 150 \text{ km s}^{-1}$. This is a common range among young to middle-aged SNRs with strong [O III] emission, but unlikely for an old remnant ~ 100 pc in diameter. Consequently, if SDO were a SNR it would likely be of moderate age and among the closest SN remnants known.

While a SNR nature for SDO is possible, there are difficulties with a SNR explanation, primarily the lack of any other portion of a supposed remnant shell. As shown in Figure 3, SDO is the only [O III] nebulosity around M31. In addition, we found no hint of a possible associated $\text{H}\alpha$ emission shell around M31 that might complete a SNR shell. In that scenario, SDO might be just one part that is especially bright in [O III] line emission. If it was a large, nearby SNR located well above the Galactic plane with low expected extinction, the lack of any $\text{H}\alpha$ or additional [O III] emission from other portions of a SNR shell would be quite unusual.

Moreover, although strong [O III] emission in SNRs is not uncommon, this type of SNR emission almost always has the morphology of sharp, thin filaments marking the remnant’s outermost shock boundary. This is not what is seen. Instead, SDO exhibits a broad structure with little evidence of limb brightening, as would be expected if it were part of a large SNR emission shell. In addition, the individual features that make up SDO do not all display the same degree of curvature. The sections closest to M31 are the most curved, with the more eastern region almost straight, with little if any curvature.

The fact that SDO’s emission faces away from the Galactic plane is also opposite from that expected if the observed emission was due to an interaction of a high-latitude remnant’s expanding shell with interstellar clouds or into the ISM’s density gradient above the disk plane. Although there are examples where a high latitude remnant’s optical emission is located farthest away from the Galactic plane (e.g., G116.6-26.1; Palaiologou et al. 2022), it is more common to find high latitude SNRs with their brightest optical emission concentrated closest to the Galactic plane (e.g., G70.0-21.5, G74.0-8.5 (Cygnus Loop), G107.0+9.0, G249.7+24.7, G275.5+18.4 (Antlia), and G354.0-33.5; Fesen et al. 2015, 2018, 2020, 2021).

Another problem is the lack of any detected nonthermal radio emission at SDO’s location. Despite numerous radio surveys of M31 and local environs, there is no reported nonthermal emission in the SDO area southeast of M31’s nucleus. In both low and high frequency radio and far infrared surveys of M31, there has been no reported adjacent SNR or any evidence of emission in M31’s halo at SDO’s location so close to M31’s disk (Graeve et al. 1981; Beck & Graeve 1982; Berkhuijsen et al. 1983, 1991; Beck et al. 1998; Berkhuijsen et al. 2003; Planck Collaboration et al. 2015; Harper et al. 2023). While SDO’s faint optical emission might suggest equally faint radio emission, the lack of any hint of coincident radio emission is a potential difficulty.

We also note the small chance of discovering a SNR at Galactic latitude $b = -22.5^\circ$ plus one so close to M31 in projection. Although several large SNRs have recently been discovered located at similar and even greater distances above the Galactic plane (Churazov et al. 2021; Becker et al. 2021; Fesen et al. 2021; Palaiologou et al. 2022), only six currently known SNRs have Galactic latitudes $|b| \geq 15^\circ$, representing less than 2% of the 306 currently known Galactic SNRs (Green et al. 2022). This rarity, combined with a projected location within just 1.5 degree of M31 and having its NE-SW structure in near alignment with M31’s disk, makes the random chance of SDO being a high latitude SNR near M31 appear quite small ($\lesssim 10^{-2}$).

Although coincidental alignments have occasionally been seen for supernova remnants⁹, the combination of finding a high latitude SNR so close to and in rough alignment with M31, whose only portion of its shell structure is dominated by [O III] emission which faces away from the Galactic plane would seem to require an unusual combination of chance occurrences.

Finally, we considered whether SDO might be an interstellar filament associated with an exceptionally large Galactic SNR or ISM bubble on the scale of several 10’s of degrees in size. Filamentary structures in the ISM are not uncommon and can span a wide range of physical and density scales. (See Hacar et al. 2022 for an in-depth review of Galactic ISM filaments.) Although interstellar filaments are commonly seen in radio, infrared and H I studies, optical/UV detections of seemingly isolated filaments are rare.

One notable exception is the straight and narrow $\text{H}\alpha$ filament some 2.5° long and located at Galactic latitude $+38^\circ$ (McCullough & Benjamin 2001). This was subsequently discovered to be part of a much larger 30° long filament best seen in GALEX images (Bracco et al. 2020). Other examples are two $\sim 2^\circ$ long synchrotron filaments also detected in $\text{H}\alpha$ (West et al. 2022). Explanations of such filamentary structures have included relic fragments of a very large and nearby SNR, a low density stellar jet, a superbubble or even parts of the Local ISM Bubble. However, none of these interstellar filaments exhibit bright [O III] but weak $\text{H}\alpha$ emission. None are as broad and diffuse in appearance as SDO.

4.1.2. A Nearby Planetary Nebula

A sharply defined and curved optical nebula lacking strong radio emission and exhibiting some filament-like structure raises the possibility of SDO being a Galac-

⁹ For example, a compact flat spectrum radio source at the center of the SNR G127.1+0.5 was initially viewed as a possible collapsed stellar remnant of the SN that produced the surrounding shell of radio emission. Given the exceedingly low probability *a priori* of finding such an object at the very center of a SNR, this source was investigated and found to be a distant radio bright galaxy (Kirshner & Chevalier 1978)

tic PN, albeit an unusually large and close one. SDSS’s morphology shown in Figures 1 and 2 bears some resemblance to that seen in a few PNe that exhibit optical emission largely on one side. The reason for their non-circular shape is their interaction with the ISM (Tweedy & Kwitter 1996; Ali et al. 2000; Sabin et al. 2010, 2012; Weidmann et al. 2016; Frew et al. 2016).

Nonetheless, a PN nature for SDSS also seems doubtful. While it is well established that PN can exhibit strong [O III] emission with values of $I(4959+5007)/I(H\alpha)$ in excess of 5 (e.g., the Ring Nebula; Hawley & Miller 1977), [O III] emission is normally more concentrated to the center of the PN and close to the CSPN than that of $H\alpha$ and [N II]. Yet we find no correlated $H\alpha$ + [N II] emission similar in strength to that of SDSS’s [O III] in our images.

The morphology, curvature, and size of the arc would require the projected radius of the nebula to be at least 2° . This makes the linear radius $r_{\text{PN}} > 0.035 \times D$ with D being the distance to the nebula. SDSS would easily be the largest PN in terms of angular size, dwarfing Sh 2-216’s record-setting radius of 0.86° . Sh 2-216, which is also currently one of the closest known PN ($D_{\text{GAIA}} = 128$ pc), with an estimated age of 660,000 years (Ziegler et al. 2009), is among the oldest and the third largest PN with a radius of 1.92 pc and a central star with $M_G = 7^m08$ (Smith 2015), just behind Ton 320’s radius of 2.69 pc (central star $M_G = 6^m95$) and the gigantic nebula Alves 1 (PN G079.8-10.2) with a radius of 5.74 pc ($M_G = 7^m19$) (all using the new GAIA distances). With a proposed radius of at least 2 to 3 degrees, this thus would position SDSS within 100 pc at most, but most likely below 50 pc.

In the largest homogeneous catalog of planetary nebulae giving statistically derived diameters by Frew et al. (2016) there are 74 PNe larger than 1 pc. From them, we selected those 38 having blue central stars detected in GAIA. As shown in Kimeswenger & Barriá (2018), only central stars with $(m_{BP} - m_{RP}) < 0$ have reliable GAIA distances. In the quick-look spectra, where available, of the Hong Kong/AAO/Strasbourg $H\alpha$ (HASH, Bojčić et al. 2017) planetary nebula database, none of them has a line ratio of $[OIII](4959+5007)/H\alpha > 1$. This sample of the oldest central stars with the largest known PNe has a mean absolute magnitude in the GAIA photometric system $M_G = 7^m08 \pm 1^m03$ with the faintest to be $M_G = 9^m58$.

This means that a potential central star for SDSS lying at the largest potential distances would have a typical apparent magnitude $m_G \approx 9^m6$, with an extreme limit of $m_G \leq 12^m0$. An examination of stars within a radius of 10° around M31 resulted in 598 stars with distances below 110 pc (note: to avoid Kerker bias the volume was stretched slightly), and magnitudes below 12^m0 listed in GAIA DR3. Only two of them have a $(m_{BP} - m_{RP}) < 0$. None of them is a white dwarf. The most recent catalog of nearby white dwarfs by Jiménez-

Esteban et al. (2023) lists 88 WD stars within this field. By far the hottest star is FBS 0050+358 with only 26kK. This finding corresponds well to the spectroscopic surveys collected recently with LAMOST (Luo et al. 2021; Lei et al. 2023) and the data collection by Geier (2020).

For expansion velocities of $30 - 50 \text{ km s}^{-1}$, typical for old planetary nebulae, the expansion age for a PN is $\tau_{\text{exp}} > (10^3 \text{ yr})D_{\text{pc}}$. A complete grid of PNe models using CLOUDY (Ferland et al. 2013) along the evolutionary tracks for stars with initial masses from 0.9 to $3 M_\odot$ (Miller Bertolami 2016) was calculated. This showed that only central stars with effective temperatures above 110kK and luminosities above $800 L_\odot$ can give an excess of $[OIII](4959+5007)/H\alpha > 2$ at radii larger than 10^{18} cm ($= 0.32 \text{ pc}$). However, even at a close distance of 5 pc, the dynamic age eliminates all progenitors with masses above $1.5 M_\odot$ using the ages along the evolutionary tracks. Moreover, none of the central stars of the sample of large old PNe derived above reaches this luminosity-temperature domain in the HRD. We conclude that such a luminous white dwarf, even if masked by a main sequence star in a binary system (e.g., UCAC2 46706450; Werner et al. 2020), would not be missed at this low distance and the complete coverage of the region by GALEX.

Similar arguments eliminate the possibility of other ionizing blue stars. Blue main sequence stars or luminous blue variables (LBV) all have at least an order of magnitude higher luminosities. Moreover, as shown in radius surface brightness diagrams, compact H II regions and massive star ejecta (MSE) are at least an order of magnitude brighter in $H\alpha$ than all PNe of similar sizes Frew et al. (e.g., their Fig. A1 in 2016). However, we would still be missing the detection in the hydrogen lines with the same morphology as our [O III] arc.

4.1.3. A Bow Shock Nebula

The curvature of the SDSS nebula suggests that it might be an interstellar bow shock preceding a fast-moving star in a nearby Galactic source. Strong shocks will be produced by stars moving at velocities ($40 - 70 \text{ km s}^{-1}$) through the ISM (Shull & Kulkarni 2023) in excess of the sound speed c_s (or magnetosonic wave speed v_m). Fast-moving OB stars with strong winds have observed arc-like features of parsec size (van Buren & McCray 1988; Mackey et al. 2016). An O-star moving at velocity $V_* = (40 \text{ km s}^{-1})V_{40}$ would produce a wind termination shock of the approximate size,

$$r_b \approx \left[\frac{\dot{M}_w V_w}{4\pi\mu n_H} \right]^{1/2} V_*^{-1} \\ \approx (1.0 \text{ pc}) \dot{M}_{-6}^{1/2} n_H^{-1/2} \left(\frac{V_w}{1000 \text{ km s}^{-1}} \right)^{1/2} V_{40}^{-1} \quad (1)$$

Here, we express the stellar mass-loss rate as $\dot{M}_w = (10^{-6} M_\odot \text{ yr}^{-1})\dot{M}_{-6}$ and equate the wind ram pres-

Table 1. Comparisons of Likelihoods of Various Origin Scenarios for the SDSO Nebula

SDSO's Properties	Galactic Nebula			M31 Nebula
	SN Remnant	Planetary Nebula	Stellar Bow Shock	Halo-CGM Shock
$V_{\text{Hel}} \sim 0 \text{ km s}^{-1}$	likely	likely	likely	unlikely
Majority of nebula with $[\text{O III}]/\text{H}\alpha > 5$	possible	unlikely	unlikely	possible
Absence of any associated $\text{H}\alpha$ emission	unlikely	unlikely	unlikely	possible
Percentage of known nebulae with $\text{Dia.} \geq 1.5^\circ$	$< 10\%^a$	$< 0.003\%^b$	$0\%^c$...
Probability of nebula at $ b > 20^\circ$	very low	very low	very low	100%
Probability of nebula within 2° of M31	very low	very low	very low	100%
Probability of an one-sided nebula	low	low	high	100%

^aGreen et al. (2022) SNR catalog.

^bFrew et al. (2016) on-line PN catalog.

^cvan Buren & McCray (1988), Cox et al. (2012), Decin et al. (2012), Peri et al. (2015).

sure, $\dot{M}_w V_w / 4\pi r^2$, with the pressure, $\rho_{\text{ISM}} V_*^2$, of the ISM of mass density $\rho_{\text{ISM}} = 1.4 m_{\text{H}} n_{\text{H}}$. At a distance $d \approx 100 \text{ kpc}$, the angular size would be $\theta_b = r_b / d \approx 10^{-2} \text{ rad}$ (0.57°), considerably smaller than the implied radius of the SDSO arc.

A bow shock could explain SDSO's limited extent and its one-sided nebula appearance. SDSO's bright [O III] emission relative to that of $\text{H}\alpha$ could signal a high stellar wind speed and/or source space velocity. Its broad morphology might arise from the projection of overlapping shock fronts due to variations in a star's mass-loss history. However, we view it unlikely that SDSO represents a stellar bow shock nebula. The huge angular size of SDSO would require a nearby star with an enormous mass-loss rate that has somehow escaped prior identification.

Optical and infrared emission bow shocks are seen in several different astrophysical settings, including mass loss from high mass OB stars of which $\simeq 25\%$ are runaway stars (van Buren & McCray 1988; Blaauw 1993; Bodensteiner et al. 2018; Chick et al. 2020), red supergiants (Noriega-Crespo et al. 1997; Meyer et al. 2014), nova-like cataclysmic variables (Castro Segura et al. 2021), pulsars (Kulkarni & Hester 1988; Brownsberger & Romani 2014), and AGB carbon stars (Libert et al. 2007; Weidmann et al. 2023). Unlike the highly curved bow shocks seen around pulsars, stars with space velocities of a few 10 's of km s^{-1} lead to much less curved nebulae like that of SDSO, not unlike that seen in the infrared nebula around the runaway O9.5 V star Zeta Oph (Green et al. 2022).

In all the cases above, the source of the wind lies close to the bow shock nebula and at the apex of the bow shock. However, ignoring the lack of expected curved bow shock geometry in SDSO, we could not identify an obvious stellar source that could generate the observed

nebula. The nearest bright optical and GALEX FUV source to SDSO is the A0 E star HD 4336 ($V = 9.01$). With a Gaia DR3 parallax of 3.02 mas implying a distance of $\simeq 330 \text{ pc}$, its luminosity, and stellar winds are far too weak to produce a photoionized bow shock with the dimensions for SDSO of around 10 pc if at a distance of around 300 pc . A bright FUV source projected farther away from SDSO is the symbiotic binary EG Andromedae ($V = 7.22$, M2.4 III + WD) (see Fig. 8) which has an estimated mass-loss rate of $\dot{M}_w \sim 10^{-6} M_\odot \text{ yr}^{-1}$. However, if SDSO was a bow shock associated with EG And, the star's Gaia DR3 estimated distance of $600 \pm 12 \text{ pc}$ would imply SDSO's physical size of roughly 15 pc , an order of magnitude larger in scale to the largest stellar bow shocks which have typical dimensions around 1 pc .

4.2. Extragalactic: A M31 Nebula

The discussions above led us to the viewpoint that a Galactic origin for SDSO is unlikely. This conclusion is supported by Table 1, where we list the likelihood of the three Galactic origin scenarios for explaining some of SDSO's observed properties. The combination of low or unlikely probabilities for each of the galactic scenarios considered, namely an unrecognized SN remnant, a planetary nebula, or a stellar bow shock, led us to consider instead a scenario where SDSO is physically related to M31 as suggested by the close projection of SDSO so near M31 in the sky despite the difference in their heliocentric velocities.

Large emission nebulae around massive galaxies showing [O III] emission lines have been detected before. The most famous case is that of Hanny's Voorwerp near the spiral galaxy IC 2497 (Lintott et al. 2009; Keel et al. 2012). However, such cases are related to the galaxy's AGN emission, something not the case for M31. Despite

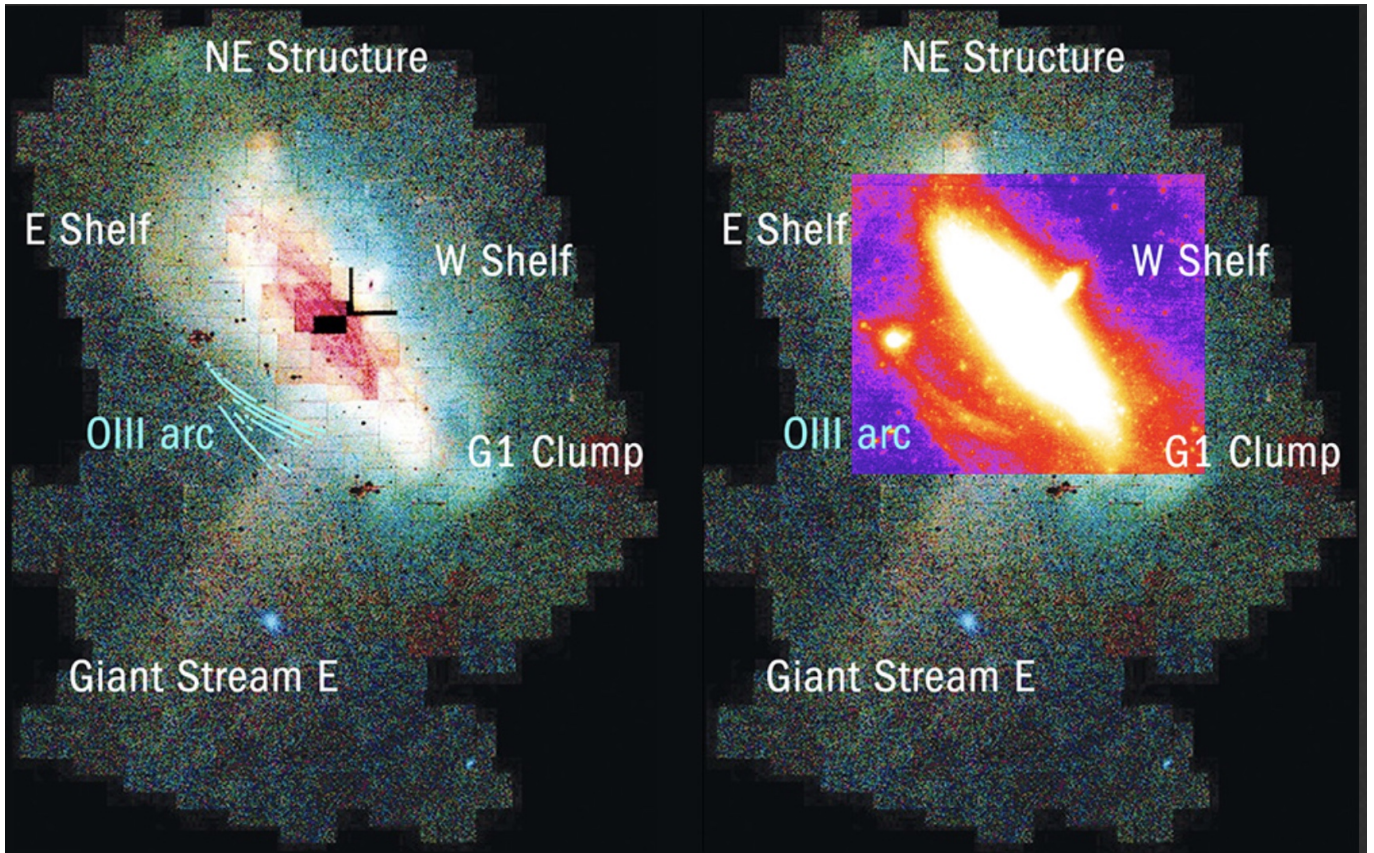


Figure 12. Location of SDO relative to M31’s stellar streams. Left Panel: Figure adapted from [McConnachie et al. \(2004\)](#) with SDO marked by several blue streaks. Right Panel: Color insert of our [O III] image overlaid on the same figure. SDO’s projected position lies in a region in between M31’s stellar streams with its westernmost extent matching at the edge of the Giant Stream East.

displaying a radial velocity more in line with a Galactic origin, the [O III] arc’s projected location so close to M31 with a lateral structure nearly parallel to M31’s disk naturally suggests a connection with M31. If the arc were physically near M31, it would have an extension of more than 100,000 light-years and would contain a substantial amount of matter.

The arc’s average offset $\sim 1.2^\circ$ on the sky from M31’s nucleus translates to a distance ($16.1 \text{ kpc} / \cos i$) from the M31 nucleus, where $i \sim 72^\circ$ is the inclination angle of M31’s disk plane. Thus, the filaments could be $\sim 70 \text{ kpc}$ away from the M31 nucleus if they lie in the disk plane.

An interaction of M31’s halo with the circumgalactic medium would seem possible, in view of the numerous tidal debris streams that lace the M31 environs and its collection of small satellite galaxies: ([Ibata et al. 2001](#); [McConnachie et al. 2003, 2005, 2018](#); [van der Marel et al. 2012](#); [Gilbert et al. 2007](#); [Ferguson & Mackey 2016](#); [Gilbert et al. 2019](#); [Fardal et al. 2007, 2012](#)). In considering possible M31-related scenarios, we examined stellar observations ([Dey et al. 2023](#)) and N-body models ([Fardal et al. 2007](#)) of stellar streams, particularly the GSS. However, the modeled trajectory of the merging galaxy and the observed blueshifted velocities of the

stars relative to M31 are inconsistent with the velocity measured for the filaments. In the model, the merging galaxy approached M31 from the far side and passed back through M31. The blue-shifted stars in the GSS are falling back toward M31. Thus, we were unable to find a consistent kinematic scenario connecting the GSS merger and the filaments.

Figure 12 shows the location of SDO relative to the major M31 streams close to the M31 disk. SDO can be seen as located east of the so-called Giant Stellar Stream (GSS) ([Ibata et al. 2001](#); [Dey et al. 2023](#)), with its southwestern extent roughly coincident with GSS’s sharp eastern edge. Because these stellar stream studies do not map the associated gas, it is possible that the gas seen in SDO might mark the locations of tidal effects differently than stripped stars, since gas is subject to dissipation and pressure gradients. Consequently, SDO may be the signature of the M31 halo interacting with relic circumgalactic gas associated with ancient tidal disruption events.

In such a scenario, the [O III] emission feature (SDO) may be a thin shield of material in the M31 halo marking interaction with local HVCs or Local Group gas. The physical scale of such an interaction would be roughly

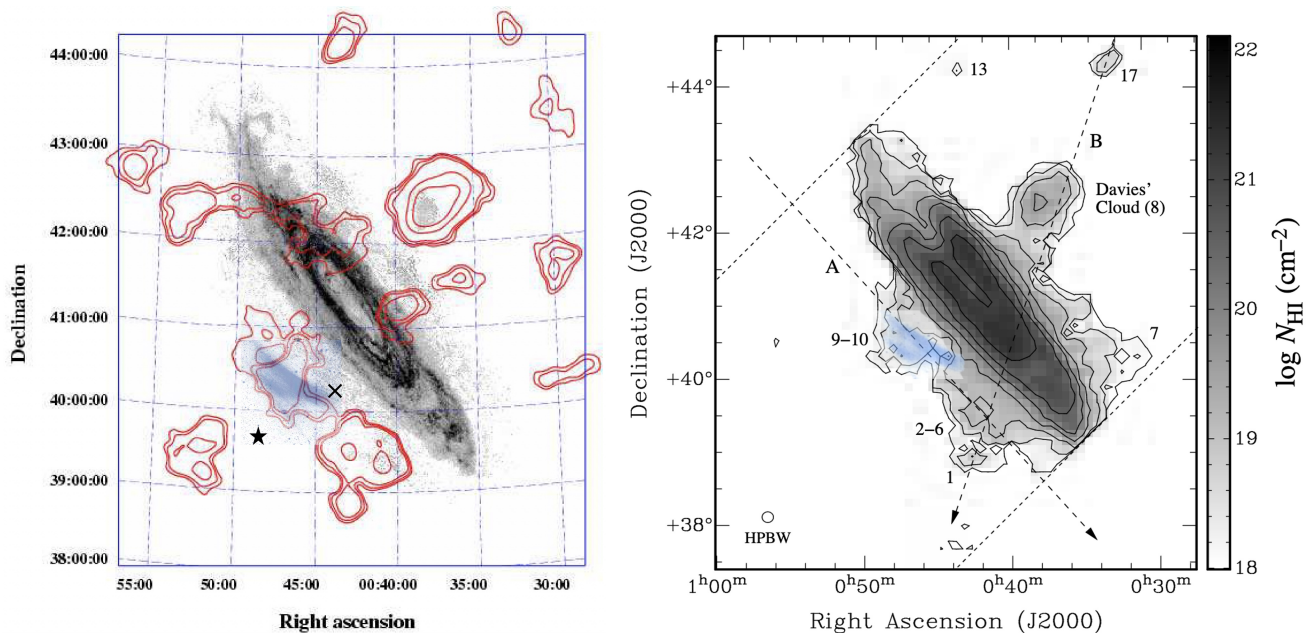


Figure 13. Location of SDO projected onto maps of high-velocity H I clouds near M31. Left panel: Map from Thilker et al. (2004, 2005a) with overlay of SDO’s [O III] emission shown in blue. The positions of quasars near SDO studied by Rao et al. (2013) and by Lehner et al. (2015) are indicated by \times and \star , respectively. SDO’s projected position coincides with an H I cloud exhibiting an elongated morphology similar to SDO’s NE-SW appearance. Right panel: H I survey map of HVCs around M31 from Westmeier et al. (2008) with SDO’s projected location again shown in blue.

the same as M31’s disk, namely a few degrees, consistent with SDO’s angular size. It would also likely display a small concave curvature, again like that of SDO. M31’s unusually high halo stellar mass fraction (Trujillo & Fliri 2016) lends additional support to this general picture.

In addition, the transverse velocity and proper motion vector of M31 vector points southeast of M31’s nucleus (van der Marel & Guhathakurta 2008; Sohn et al. 2012; van der Marel et al. 2012; Salomon et al. 2021). This places it perpendicular to and passing through the SDO filaments. In such an interaction model, the southeastern boundary of the M31’s halo can be considered as the “leading edge” of M31’s Local Group motion.

The coincidence of SDO’s projected location with M31’s motion is consistent with the possibility of an interaction between M31 and its HVCs or circumgalactic medium (CGM). However, while a velocity of M31 relative to the Milky Way of around 100 km s^{-1} could generate a shock bright in [O III], it is not obvious how such an interaction is consistent with the low ($-10 \pm 7 \text{ km s}^{-1}$) heliocentric velocity that we measure.

Interestingly, some of the intergalactic gas around M31 is believed to be from a tidal encounter between M31 and M33 some 1-3 Gyr ago (Blitz et al. 1999; Braun & Thilker 2004; Bekki 2008). This left a discontinuous stream of H I clouds between the two galaxies as reported by Braun & Thilker (2004) and Thilker et al. (2004) and subsequently confirmed and investigated by Lockman et al. (2012), Westmeier et al. (2008), Wolfe et al. (2013), and Kerp et al. (2016).

Figure 13 shows the location of high velocity clouds around M31 reported by Thilker et al. (2004, 2005a) and Westmeier et al. (2008) thought to be the equivalent to the Milky Way’s HVCs. The location of SDO matches one of these HVCs southeast of the M31 nucleus with a projected location coincident with one of these clouds and exhibiting a morphology similar to that cloud’s NE-SW elongation. However, the heliocentric velocity of this HVC is -175 km s^{-1} , far from SDO’s -10 km s^{-1} value.

Such H I studies of HVCs near M31 typically only survey radial velocities from -100 to -600 km s^{-1} and are hence blind to low velocity gas. However, a study of H I clouds near M31 by Kerp et al. (2016) covered velocities down to -25 km s^{-1} with an angular resolution of $10.8'$. While detecting no significant low velocity H I gas at SDO’s location, the curved M31-M33 stream of HVCs aligns with SDO’s location off M31.

We note that Rao et al. (2013) and Lehner et al. (2020) analyzed low-dispersion UV spectra taken with the Cosmic Origins Spectrograph on *Hubble Space Telescope* to explore the CGM around M31, using metal absorption lines toward background quasars. However, the velocities seen, relative to the core of M31 are fairly small. The locations of two of these quasars are shown in the left panel of Figure 13. The sight-line to one of the Rao et al. (2013) targets, 0043+4016, is coincident with very faint SDO’s [O III] emission along its northern limb (shown in the figure as an \times symbol). However, strong line blending and low spectral resolution of the

Si II $\lambda 1260$ and C IV $\lambda 1548$ features limited a clear HVC detection.

A second target from the [Lehner et al. \(2015\)](#) list, RX J0048.3+3941, is located 1.9° from the M31 core and about $20'$ outside our arc-like features (shown in the figure as a \star symbol). [Lehner et al. \(2020\)](#) detected absorption lines from ionized metals (C II, Si III, Si IV, C IV) at LSR velocities between -170 km s^{-1} and -300 km s^{-1} , similar to that of the H I cloud. They interpret these ionized absorption features as gas in the CGM of M31. However, as shown in Figure 13, the quasar sight line does not pass through the 21-cm contours of the H I cloud. On the other hand, Galactic HVCs and clouds in the CGM are expected to be ionized and could extend well beyond the H I contours.

While positional coincidences of SDSO with M31's circumgalactic H I clouds are suggestive, we do not know the 3D location of SDSO relative to the high (or low) velocity H I emission clouds. Assuming that SDSO represents shocked halo gas or CGM at roughly M31's 770 kpc distance, we can estimate some of its basic properties. For filaments extending over 900 arcmin^2 ($15' \times 60'$) with surface brightness I_{arc} scaled to 0.1 Rayleigh, the radiated luminosity is $(1.7 \times 10^{38} \text{ erg s}^{-1})(I_{\text{arc}}/0.1 \text{ R})$. We assume that the [O III] is the dominant ionization state of oxygen in collisionally excited gas at $T \approx 10^4 \text{ K}$, with $\lambda 5007$ collision strength $\Omega_{12} = 2.19$, hydrogen density $n_{\text{H}} \approx 10^{-2} \text{ cm}^{-3}$, and metallicity Z relative to the solar oxygen abundance $(n_{\text{O}}/n_{\text{H}})_{\odot} = 5.62 \times 10^{-4}$. From the observed surface brightness, we compute a volume emission measure,

$$\text{EM} \equiv n_{\text{H}}^2 V_{\text{arc}} = (6.55 \times 10^{61} \text{ cm}^{-3}) \left[\frac{I_{\text{arc}}}{0.1 \text{ R}} \right] \left[\frac{Z}{Z_{\odot}} \right]^{-1}, \quad (2)$$

and a mass ($1.4n_{\text{H}}m_{\text{H}}V_{\text{arc}}$) of

$$M_{\text{arc}} \approx (8 \times 10^6 M_{\odot}) \left[\frac{I_{\text{arc}}}{0.1 \text{ R}} \right] \left[\frac{Z}{Z_{\odot}} \right]^{-1} \left[\frac{0.01 \text{ cm}^{-3}}{n_{\text{H}}} \right]. \quad (3)$$

We scaled the uncertain density in the filaments to $n_{\text{H}} = 0.01 \text{ cm}^{-3}$, typical of Galactic HVC densities ([Collins et al. 2007](#)). This density is consistent with a rough estimate (0.004 cm^{-3}) from the emission measure, assuming that the filaments have a depth of $15'$ comparable to their radial extent on the sky. Such densities would allow the gas to cool on dynamic time scales for 100 km s^{-1} tidally stripped outflows across 50–100 kpc distances.

5. CONCLUSIONS

The presence of an exceedingly faint nebulosity (SDSO) strong in [O III] emission within 1.2° of M31 was an unexpected discovery made through the addition of hundreds of exposures taken by amateur astronomers using small telescopes equipped with narrow, high throughput passband filters and sensitive digital

detectors. Here we presented images that better defined the nebula's extent and structure, plus radial velocity results from low-dispersion spectra. A summary of our main results and findings follows:

1) Deep [O III] images show SDSO to be composed of diffuse emission streaks up to 2° in length. Deep $\text{H}\alpha$ images reveal no strong coincident emission, suggesting a high ratio of $I([\text{O III}] \lambda\lambda 4959, 5007)/I(\text{H}\alpha)$.

2) We find no other [O III] emission nebulosity as bright as SDSO within several degrees of M31, and no filamentary $\text{H}\alpha$ emission that might be connected to SDSO. We also find no far UV emission coincident with SDSO in GALEX images.

3) Long slit, low-dispersion optical spectra taken at two locations along the arc's northern edge reveal faint [O III] emission matching the location and extent of emission seen in our [O III] images. Because this emission vanishes outside the nebulosity seen in our images, we are confident that we have detected emission from SDSO. We estimate a heliocentric velocity of $-9.8 \pm 6.8 \text{ km s}^{-1}$.

4) The surface brightness of SDSO's brighter regions ranges from $(2.5 - 4.0) \times 10^{-18} \text{ erg s}^{-1} \text{ cm}^{-2} \text{ arcsec}^{-2}$. These values are consistent with the earlier estimate reported in [Drechsler et al. \(2023\)](#). SDSO's brighter regions have a surface brightness of ~ 0.55 Rayleigh, with the faintest regions in our [O III] images detected at ~ 0.2 Rayleigh.

5) Because of SDSO's low radial velocity, we have considered various possible Galactic origins for this strong [O III] but weak $\text{H}\alpha$ emission nebula. We conclude that a supernova remnant, nearby planetary nebula, or stellar bow shock nebula explanations for its origin are all unlikely. Instead, we favor an extragalactic origin involving interaction of M31's outer halo with a circumgalactic high velocity cloud leading to shock emission. This cloud may be related to a large and ancient stream of discrete H I clouds between M33 and M31 that might be the result of a past tidal disruption event.

We note that our path to favoring an extragalactic halo-cloud interaction scenario was not a straight one. Initially, SDSO's low radial velocity seemed to be clear evidence for it being a Galactic nebula. But no Galactic nebula scenario seemed to fit, whereas SDSO's emission properties and positional coincidences in line with an extragalactic scenario were hard to dismiss. These included its visibility in [O III] but not in $\text{H}\alpha$, its broad and largely diffuse emission structure despite its strong [O III] line emission, its apparent isolation from other $\text{H}\alpha$ and [O III] nebulae in this region of the sky, its alignment with and proximity to M31's disk, the lack of any potential ionizing Galactic sources in this direction, its location southeast of M31's nucleus consistent with the galaxy's transverse velocity and proper motion vector with its NE-SW structure nearly perpendicular to this motion, and its projected coincidence with an H I

cloud near M31 with which it shares a similar NE-SW alignment. None of these by themselves are very persuasive, but viewed together they make a good case for an extragalactic origin.

There are a number of follow-up observations that could help resolve the true nature and origin of the SDSO nebulosity. Although we are confident in our radial velocity measurement, our result and that of [Amram et al. \(2023\)](#) were obtained with low dispersion spectra. Higher resolution spectra would be especially useful to investigate its radial velocity across SDSO's whole structure. Spectra covering several emission lines including [O I] $\lambda\lambda 6300, 6364$, [O II] $\lambda\lambda 3726, 3729$, [O III] $\lambda\lambda 4959, 5007$, [N II] $\lambda\lambda 6548, 6583$, [S II] $\lambda\lambda 6716, 6731$, H α , and H β could provide valuable data on the nebula's density and ionization state. Sensitive radio observations could also provide a test for the shock scenario as the origin of the SDSO's strong [O III] emission through the detection of nonthermal radio emission. Finally, sensitive and high resolution 21 cm data of the H I emission cloud coincident with SDSO and covering the velocity range of -10 to -100 km s $^{-1}$ could investigate the presence of low velocity gas at SDSO's exact location as we have proposed.

We thank Arjun Dey, Mark Fardal, Gary Ferland, Andrew Fox, and Wolfgang Reich for helpful comments and conversations about the SDSO nebula and M31's stellar streams. We are grateful to Eric Galayda and the entire MDM staff for making the optical spectral observations possible. We also thank Andrew Fryhover, Vicent Peris, and Alicia Lozano for generously making available their deep H α images of M31. This work made use of the Simbad database, NASA's Skyview online data archives, the Max Planck Institute for Radio Astronomy Survey Sampler, and the Gaia EDR3 catalog.

Facilities: MDM Observatory (OSMOS), and various privately owned and operated telescopes

Software: PYRAF (Science Software Branch at STScI 2012), Astropy v4.0 (Astropy Collaboration et al. 2013), ds9 (Smithsonian Astrophysical Observatory 2000), L.A. Cosmic (van Dokkum 2001), ESO-MIDAS (Warmels 1992)

REFERENCES

- Abraham, R. G., & van Dokkum, P. G. 2014, *PASP*, 126, 55, doi: [10.1086/674875](#)
- Ali, A., El-Nawawy, M. S., & Pfeleiderer, J. 2000, *Ap&SS*, 271, 245, doi: [10.1023/A:1002442632274](#)
- Amram, P., Adami, C., Epinat, B., & Chemin, L. 2023, *A&A*, 671, L13, doi: [10.1051/0004-6361/202346311](#)
- Astropy Collaboration, Robitaille, T. P., Tollerud, E. J., et al. 2013, *A&A*, 558, A33, doi: [10.1051/0004-6361/201322068](#)
- Beck, R., Berkhuijsen, E. M., & Hoernes, P. 1998, *A&AS*, 129, 329, doi: [10.1051/aas:1998187](#)
- Beck, R., & Graeve, R. 1982, *A&A*, 105, 192
- Becker, W., Hurley-Walker, N., Weinberger, C., et al. 2021, *A&A*, 648, A30, doi: [10.1051/0004-6361/202040156](#)
- Bekki, K. 2008, *MNRAS*, 390, L24, doi: [10.1111/j.1745-3933.2008.00528.x](#)
- Berkhuijsen, E. M., Beck, R., & Hoernes, P. 2003, *A&A*, 398, 937, doi: [10.1051/0004-6361:20021710](#)
- Berkhuijsen, E. M., Golla, G., & Beck, R. 1991, in *The Interstellar Disk-Halo Connection in Galaxies*, ed. H. Bloemen, Vol. 144, 233
- Berkhuijsen, E. M., Wielebinski, R., & Beck, R. 1983, *A&A*, 117, 141
- Bianchi, L., Kang, Y., Hodge, P., Dalcanton, J., & Williams, B. 2014, *Advances in Space Research*, 53, 928, doi: [10.1016/j.asr.2013.08.024](#)
- Blaauw, A. 1993, in *Astronomical Society of the Pacific Conference Series*, Vol. 35, *Massive Stars: Their Lives in the Interstellar Medium*, ed. J. P. Cassinelli & E. B. Churchwell, 207
- Blair, W. P., Sawyer, D. L., Kirshner, R. P., Gull, T. R., & Parker, R. A. R. 1980, *ApJ*, 242, 592, doi: [10.1086/158494](#)
- Blitz, L., Spergel, D. N., Teuben, P. J., Hartmann, D., & Burton, W. B. 1999, *ApJ*, 514, 818, doi: [10.1086/306963](#)
- Bodensteiner, J., Baade, D., Greiner, J., & Langer, N. 2018, *A&A*, 618, A110, doi: [10.1051/0004-6361/201832722](#)
- Bojičić, I. S., Parker, Q. A., & Frew, D. J. 2017, in *Planetary Nebulae: Multi-Wavelength Probes of Stellar and Galactic Evolution*, ed. X. Liu, L. Stanghellini, & A. Karakas, Vol. 323, 327–328, doi: [10.1017/S1743921317003234](#)
- Boumis, P., Meaburn, J., López, J. A., et al. 2004, *A&A*, 424, 583, doi: [10.1051/0004-6361:20040410](#)
- Bracco, A., Benjamin, R. A., Alves, M. I. R., et al. 2020, *A&A*, 636, L8, doi: [10.1051/0004-6361/202037975](#)
- Braun, R., & Thilker, D. A. 2004, *A&A*, 417, 421, doi: [10.1051/0004-6361:20034423](#)
- Brownsberger, S., & Romani, R. W. 2014, *ApJ*, 784, 154, doi: [10.1088/0004-637X/784/2/154](#)
- Bruhweiler, F. C., Gull, T. R., Henize, K. G., & Cannon, R. D. 1981, *ApJ*, 251, 126, doi: [10.1086/159446](#)

- Castro Segura, N., Knigge, C., Acosta-Pulido, J. A., et al. 2021, *MNRAS*, 501, 1951, doi: [10.1093/mnras/staa2516](https://doi.org/10.1093/mnras/staa2516)
- Chick, W. T., Kobulnicky, H. A., Schurhammer, D. P., et al. 2020, *ApJS*, 251, 29, doi: [10.3847/1538-4365/abc0e5](https://doi.org/10.3847/1538-4365/abc0e5)
- Chu, Y. H. 1981, *ApJ*, 249, 195, doi: [10.1086/159275](https://doi.org/10.1086/159275)
- Churazov, E. M., Khabibullin, I. I., Bykov, A. M., et al. 2021, *MNRAS*, 507, 971, doi: [10.1093/mnras/stab2125](https://doi.org/10.1093/mnras/stab2125)
- Collins, J. A., Shull, J. M., & Giroux, M. L. 2007, *ApJ*, 657, 271, doi: [10.1086/510770](https://doi.org/10.1086/510770)
- Cox, N. L. J., Kerschbaum, F., van Marle, A. J., et al. 2012, *A&A*, 537, A35, doi: [10.1051/0004-6361/201117910](https://doi.org/10.1051/0004-6361/201117910)
- de Vaucouleurs, G. 1958, *ApJ*, 128, 465, doi: [10.1086/146564](https://doi.org/10.1086/146564)
- de Vaucouleurs, G., de Vaucouleurs, A., Corwin, Herold G., J., et al. 1991, *Third Reference Catalogue of Bright Galaxies*
- Decin, L., Cox, N. L. J., Royer, P., et al. 2012, *A&A*, 548, A113, doi: [10.1051/0004-6361/201219792](https://doi.org/10.1051/0004-6361/201219792)
- Dennison, B., Simonetti, J. H., & Topasna, G. A. 1998, *PASA*, 15, 147, doi: [10.1071/AS98147](https://doi.org/10.1071/AS98147)
- Dey, A., Najita, J. R., Kuposov, S. E., et al. 2023, *ApJ*, 944, 1, doi: [10.3847/1538-4357/aca5f8](https://doi.org/10.3847/1538-4357/aca5f8)
- Drechsler, M., Strottner, X., Sainty, Y., et al. 2023, *Research Notes of the American Astronomical Society*, 7, 1, doi: [10.3847/2515-5172/acaf7e](https://doi.org/10.3847/2515-5172/acaf7e)
- Drew, J. E., Greimel, R., Irwin, M. J., et al. 2005, *MNRAS*, 362, 753, doi: [10.1111/j.1365-2966.2005.09330.x](https://doi.org/10.1111/j.1365-2966.2005.09330.x)
- Duncan, A. R., Stewart, R. T., Haynes, R. F., & Jones, K. L. 1995, *MNRAS*, 277, 36, doi: [10.1093/mnras/277.1.36](https://doi.org/10.1093/mnras/277.1.36)
- Fardal, M. A., Guhathakurta, P., Babul, A., & McConnachie, A. W. 2007, *MNRAS*, 380, 15, doi: [10.1111/j.1365-2966.2007.11929.x](https://doi.org/10.1111/j.1365-2966.2007.11929.x)
- Fardal, M. A., Guhathakurta, P., Gilbert, K. M., et al. 2012, *MNRAS*, 423, 3134, doi: [10.1111/j.1365-2966.2012.21094.x](https://doi.org/10.1111/j.1365-2966.2012.21094.x)
- Ferguson, A. M. N., & Mackey, A. D. 2016, in *Astrophysics and Space Science Library*, Vol. 420, *Tidal Streams in the Local Group and Beyond*, ed. H. J. Newberg & J. L. Carlin, 191, doi: [10.1007/978-3-319-19336-6_8](https://doi.org/10.1007/978-3-319-19336-6_8)
- Ferland, G. J., Porter, R. L., van Hoof, P. A. M., et al. 2013, *RMxAA*, 49, 137. <https://arxiv.org/abs/1302.4485>
- Fesen, R. A., Blair, W. P., & Gull, T. R. 1981a, *ApJ*, 245, 131, doi: [10.1086/158793](https://doi.org/10.1086/158793)
- Fesen, R. A., Blair, W. P., & Kirshner, R. P. 1985, *ApJ*, 292, 29, doi: [10.1086/163130](https://doi.org/10.1086/163130)
- Fesen, R. A., Blair, W. P., Kirshner, R. P., Gull, T. R., & Parker, R. A. R. 1981b, *ApJ*, 247, 148, doi: [10.1086/159021](https://doi.org/10.1086/159021)
- Fesen, R. A., & Gull, T. R. 1983, *PASP*, 95, 196, doi: [10.1086/131144](https://doi.org/10.1086/131144)
- Fesen, R. A., Gull, T. R., & Ketelsen, D. A. 1983, *ApJS*, 51, 337, doi: [10.1086/190853](https://doi.org/10.1086/190853)
- Fesen, R. A., & Hurford, A. P. 1996, *ApJS*, 106, 563, doi: [10.1086/192348](https://doi.org/10.1086/192348)
- Fesen, R. A., Neustadt, J. M. M., Black, C. S., & Koepfel, A. H. D. 2015, *ApJ*, 812, 37, doi: [10.1088/0004-637X/812/1/37](https://doi.org/10.1088/0004-637X/812/1/37)
- Fesen, R. A., Weil, K. E., Cisneros, I. A., Blair, W. P., & Raymond, J. C. 2018, *MNRAS*, 481, 1786, doi: [10.1093/mnras/sty2370](https://doi.org/10.1093/mnras/sty2370)
- Fesen, R. A., Winkler, F., Rathore, Y., et al. 1997, *AJ*, 113, 767, doi: [10.1086/118297](https://doi.org/10.1086/118297)
- Fesen, R. A., Weil, K. E., Raymond, J. C., et al. 2020, *MNRAS*, 498, 5194, doi: [10.1093/mnras/staa2765](https://doi.org/10.1093/mnras/staa2765)
- Fesen, R. A., Drechsler, M., Weil, K. E., et al. 2021, *ApJ*, 920, 90, doi: [10.3847/1538-4357/ac0ada](https://doi.org/10.3847/1538-4357/ac0ada)
- Frew, D. J., Parker, Q. A., & Bojčić, I. S. 2016, *MNRAS*, 455, 1459, doi: [10.1093/mnras/stv1516](https://doi.org/10.1093/mnras/stv1516)
- Gaustad, J. E., McCullough, P. R., Rosing, W., & Van Buren, D. 2001, *PASP*, 113, 1326, doi: [10.1086/323969](https://doi.org/10.1086/323969)
- Geier, S. 2020, *A&A*, 635, A193, doi: [10.1051/0004-6361/202037526](https://doi.org/10.1051/0004-6361/202037526)
- Gilbert, K. M., Kirby, E. N., Escala, I., et al. 2019, *ApJ*, 883, 128, doi: [10.3847/1538-4357/ab3807](https://doi.org/10.3847/1538-4357/ab3807)
- Gilbert, K. M., Fardal, M., Kalirai, J. S., et al. 2007, *ApJ*, 668, 245, doi: [10.1086/521094](https://doi.org/10.1086/521094)
- Gilhuly, C., Merritt, A., Abraham, R., et al. 2022, *ApJ*, 932, 44, doi: [10.3847/1538-4357/ac6750](https://doi.org/10.3847/1538-4357/ac6750)
- Graeve, R., Emerson, D. T., & Wielebinski, R. 1981, *A&A*, 98, 260
- Green, S., Mackey, J., Kavanagh, P., et al. 2022, *A&A*, 665, A35, doi: [10.1051/0004-6361/202243531](https://doi.org/10.1051/0004-6361/202243531)
- Gull, T. R., Kirshner, R. P., & Parker, R. A. R. 1977, *ApJL*, 215, L69, doi: [10.1086/182480](https://doi.org/10.1086/182480)
- Gull, T. R., & Sofia, S. 1979, *ApJ*, 230, 782, doi: [10.1086/157137](https://doi.org/10.1086/157137)
- Gum, C. S. 1953, *The Observatory*, 73, 123
- . 1955, *MmRAS*, 67, 155
- Hacar, A., Clark, S., Heitsch, F., et al. 2022, *arXiv e-prints*, arXiv:2203.09562, doi: [10.48550/arXiv.2203.09562](https://doi.org/10.48550/arXiv.2203.09562)
- Haffner, L. M., Reynolds, R. J., Tufte, S. L., et al. 2003, *ApJS*, 149, 405, doi: [10.1086/378850](https://doi.org/10.1086/378850)
- Hailey, C. J., & Craig, W. W. 1994, *ApJ*, 434, 635, doi: [10.1086/174765](https://doi.org/10.1086/174765)
- Harper, S. E., Barr, A., Dickinson, C., et al. 2023, *arXiv e-prints*, arXiv:2304.03875, doi: [10.48550/arXiv.2304.03875](https://doi.org/10.48550/arXiv.2304.03875)

- Hawley, S. A., & Miller, J. S. 1977, *ApJ*, 212, 94, doi: [10.1086/155023](https://doi.org/10.1086/155023)
- Heckathorn, J. N., Bruhweiler, F. C., & Gull, T. R. 1982a, *ApJ*, 252, 230, doi: [10.1086/159550](https://doi.org/10.1086/159550)
- Heckathorn, J. N., Fesen, R. A., & Gull, T. R. 1982b, *A&A*, 114, 414
- How, T. G., Fesen, R. A., Neustadt, J. M. M., Black, C. S., & Outters, N. 2018, *MNRAS*, 478, 1987, doi: [10.1093/mnras/sty1007](https://doi.org/10.1093/mnras/sty1007)
- Ibata, R., Irwin, M., Lewis, G., Ferguson, A. M. N., & Tanvir, N. 2001, *Nature*, 412, 49, doi: [10.1038/35083506](https://doi.org/10.1038/35083506)
- Jiménez-Esteban, F. M., Torres, S., Rebassa-Mansergas, A., et al. 2023, *MNRAS*, 518, 5106, doi: [10.1093/mnras/stac3382](https://doi.org/10.1093/mnras/stac3382)
- Jones, A., Noll, S., Kausch, W., et al. 2019, *A&A*, 624, A39, doi: [10.1051/0004-6361/201833759](https://doi.org/10.1051/0004-6361/201833759)
- Kang, Y., Bianchi, L., & Rey, S.-C. 2009, *ApJ*, 703, 614, doi: [10.1088/0004-637X/703/1/614](https://doi.org/10.1088/0004-637X/703/1/614)
- Kang, Y., Rey, S.-C., Bianchi, L., et al. 2012, *ApJS*, 199, 37, doi: [10.1088/0067-0049/199/2/37](https://doi.org/10.1088/0067-0049/199/2/37)
- Keel, W. C., Lintott, C. J., Schawinski, K., et al. 2012, *AJ*, 144, 66, doi: [10.1088/0004-6256/144/2/66](https://doi.org/10.1088/0004-6256/144/2/66)
- Kerp, J., Kalberla, P. M. W., Ben Bekhti, N., et al. 2016, *A&A*, 589, A120, doi: [10.1051/0004-6361/201526395](https://doi.org/10.1051/0004-6361/201526395)
- Kim, I.-J., Seon, K.-I., Lim, Y.-M., et al. 2014, *ApJ*, 784, 12, doi: [10.1088/0004-637X/784/1/12](https://doi.org/10.1088/0004-637X/784/1/12)
- Kimeswenger, S., & Barría, D. 2018, *A&A*, 616, L2, doi: [10.1051/0004-6361/201833647](https://doi.org/10.1051/0004-6361/201833647)
- Kimeswenger, S., Thorstensen, J. R., Fesen, R. A., et al. 2021, *A&A*, 656, A145, doi: [10.1051/0004-6361/202039787](https://doi.org/10.1051/0004-6361/202039787)
- Kirshner, R. P., & Chevalier, R. A. 1978, *Nature*, 276, 480, doi: [10.1038/276480a0](https://doi.org/10.1038/276480a0)
- Kirshner, R. P., Gull, T. R., & Parker, R. A. R. 1978, *A&AS*, 31, 261
- Kronberger, M., Jacoby, G. H., Harmer, D., & Patchick, D. 2014a, in *Asymmetrical Planetary Nebulae VI Conference*, ed. C. Morisset, G. Delgado-Inglada, & S. Torres-Peimbert, 47
- Kronberger, M., Jacoby, G. H., Acker, A., et al. 2014b, in *Asymmetrical Planetary Nebulae VI Conference*, ed. C. Morisset, G. Delgado-Inglada, & S. Torres-Peimbert, 48
- Kulkarni, S. R., & Hester, J. J. 1988, *Nature*, 335, 801, doi: [10.1038/335801a0](https://doi.org/10.1038/335801a0)
- Langston, G., Minter, A., D'Addario, L., et al. 2000, *AJ*, 119, 2801, doi: [10.1086/301382](https://doi.org/10.1086/301382)
- Le Dù, P., Mulato, L., Parker, Q. A., et al. 2022, *A&A*, 666, A152, doi: [10.1051/0004-6361/202243393](https://doi.org/10.1051/0004-6361/202243393)
- Leahy, D. A., Postma, J., Buick, M., et al. 2021, *Journal of Astrophysics and Astronomy*, 42, 84, doi: [10.1007/s12036-020-09682-3](https://doi.org/10.1007/s12036-020-09682-3)
- Lehner, N., Howk, J. C., & Wakker, B. P. 2015, *ApJ*, 804, 79, doi: [10.1088/0004-637X/804/2/79](https://doi.org/10.1088/0004-637X/804/2/79)
- Lehner, N., Berek, S. C., Howk, J. C., et al. 2020, *ApJ*, 900, 9, doi: [10.3847/1538-4357/aba49c](https://doi.org/10.3847/1538-4357/aba49c)
- Lei, Z., He, R., Németh, P., et al. 2023, *ApJ*, 942, 109, doi: [10.3847/1538-4357/aca542](https://doi.org/10.3847/1538-4357/aca542)
- Libert, Y., Gérard, E., & Le Bertre, T. 2007, *MNRAS*, 380, 1161, doi: [10.1111/j.1365-2966.2007.12154.x](https://doi.org/10.1111/j.1365-2966.2007.12154.x)
- Lintott, C. J., Schawinski, K., Keel, W., et al. 2009, *MNRAS*, 399, 129, doi: [10.1111/j.1365-2966.2009.15299.x](https://doi.org/10.1111/j.1365-2966.2009.15299.x)
- Lockman, F. J., Free, N. L., & Shields, J. C. 2012, *AJ*, 144, 52, doi: [10.1088/0004-6256/144/2/52](https://doi.org/10.1088/0004-6256/144/2/52)
- Luo, Y., Németh, P., Wang, K., Wang, X., & Han, Z. 2021, *ApJS*, 256, 28, doi: [10.3847/1538-4365/ac11f6](https://doi.org/10.3847/1538-4365/ac11f6)
- Mackey, J., Haworth, T. J., Gvaramadze, V. V., et al. 2016, *A&A*, 586, A114, doi: [10.1051/0004-6361/201527569](https://doi.org/10.1051/0004-6361/201527569)
- Madore, B. F. 2005, in *American Institute of Physics Conference Series*, Vol. 761, *The Spectral Energy Distributions of Gas-Rich Galaxies: Confronting Models with Data*, ed. C. C. Popescu & R. J. Tuffs, 331–343, doi: [10.1063/1.1913948](https://doi.org/10.1063/1.1913948)
- Martinez-Delgado, D. 2020, arXiv e-prints, arXiv:2001.05746, doi: [10.48550/arXiv.2001.05746](https://doi.org/10.48550/arXiv.2001.05746)
- Martini, P., Stoll, R., Derwent, M. A., et al. 2011, *PASP*, 123, 187, doi: [10.1086/658357](https://doi.org/10.1086/658357)
- Mavromatakis, F., Boumis, P., Papamastorakis, J., & Ventura, J. 2002, *A&A*, 388, 355, doi: [10.1051/0004-6361:20020511](https://doi.org/10.1051/0004-6361:20020511)
- McConnachie, A., Ferguson, A., Huxor, A., et al. 2004, *The Newsletter of the Isaac Newton Group of Telescopes*, 8, 8
- McConnachie, A. W., Irwin, M. J., Ferguson, A. M. N., et al. 2005, *MNRAS*, 356, 979, doi: [10.1111/j.1365-2966.2004.08514.x](https://doi.org/10.1111/j.1365-2966.2004.08514.x)
- McConnachie, A. W., Irwin, M. J., Ibata, R. A., et al. 2003, *MNRAS*, 343, 1335, doi: [10.1046/j.1365-8711.2003.06785.x](https://doi.org/10.1046/j.1365-8711.2003.06785.x)
- McConnachie, A. W., Ibata, R., Martin, N., et al. 2018, *ApJ*, 868, 55, doi: [10.3847/1538-4357/aae8e7](https://doi.org/10.3847/1538-4357/aae8e7)
- McCullough, P. R., & Benjamin, R. A. 2001, *AJ*, 122, 1500, doi: [10.1086/322097](https://doi.org/10.1086/322097)
- Meyer, D. M. A., Gvaramadze, V. V., Langer, N., et al. 2014, *MNRAS*, 439, L41, doi: [10.1093/mnras/slt176](https://doi.org/10.1093/mnras/slt176)
- Miller Bertolami, M. M. 2016, *A&A*, 588, A25, doi: [10.1051/0004-6361/201526577](https://doi.org/10.1051/0004-6361/201526577)
- Minkowski, R. 1946, *PASP*, 58, 305, doi: [10.1086/125855](https://doi.org/10.1086/125855)
- . 1947, *PASP*, 59, 257, doi: [10.1086/125962](https://doi.org/10.1086/125962)
- . 1948, *PASP*, 60, 386, doi: [10.1086/126101](https://doi.org/10.1086/126101)

- Morgan, W. W., Strömgren, B., & Johnson, H. M. 1955, *ApJ*, 121, 611, doi: [10.1086/146026](https://doi.org/10.1086/146026)
- Morrissey, P., Conrow, T., Barlow, T. A., et al. 2007, *ApJS*, 173, 682, doi: [10.1086/520512](https://doi.org/10.1086/520512)
- Noll, S., Kausch, W., Barden, M., et al. 2012, *A&A*, 543, A92, doi: [10.1051/0004-6361/201219040](https://doi.org/10.1051/0004-6361/201219040)
- Noll, S., Kimeswenger, S., Proxauf, B., et al. 2017, *Journal of Atmospheric and Solar-Terrestrial Physics*, 163, 54, doi: [10.1016/j.jastp.2017.05.012](https://doi.org/10.1016/j.jastp.2017.05.012)
- Noriega-Crespo, A., van Buren, D., Cao, Y., & Dgani, R. 1997, *AJ*, 114, 837, doi: [10.1086/118517](https://doi.org/10.1086/118517)
- Palaiologou, E. V., Leonidaki, I., & Kopsacheili, M. 2022, *MNRAS*, 515, 339, doi: [10.1093/mnras/stac1599](https://doi.org/10.1093/mnras/stac1599)
- Parker, Q. A., Phillipps, S., Pierce, M. J., et al. 2005, *MNRAS*, 362, 689, doi: [10.1111/j.1365-2966.2005.09350.x](https://doi.org/10.1111/j.1365-2966.2005.09350.x)
- Parker, R. A. R., Gull, T. R., & Kirshner, R. P. 1979, *An emission-line survey of the Milky Way*, Vol. 434
- Peri, C. S., Benaglia, P., & Isequilla, N. L. 2015, *A&A*, 578, A45, doi: [10.1051/0004-6361/201424676](https://doi.org/10.1051/0004-6361/201424676)
- Planck Collaboration, Ade, P. A. R., Aghanim, N., et al. 2015, *A&A*, 582, A28, doi: [10.1051/0004-6361/201424643](https://doi.org/10.1051/0004-6361/201424643)
- Rao, S. M., Sardane, G., Turnshek, D. A., et al. 2013, *MNRAS*, 432, 866, doi: [10.1093/mnras/stt417](https://doi.org/10.1093/mnras/stt417)
- Reich, W., Fuerst, E., Reich, P., & Reif, K. 1990, *A&AS*, 85, 633
- Sabin, L., Corradi, R. L. M., Parker, Q., Mampaso, A., & Zijlstra, A. 2012, *IAU Symposium*, 283, 492, doi: [10.1017/S1743921312012082](https://doi.org/10.1017/S1743921312012082)
- Sabin, L., Zijlstra, A. A., Wareing, C., et al. 2010, *PASA*, 27, 166, doi: [10.1071/AS09046](https://doi.org/10.1071/AS09046)
- Salomon, J. B., Ibata, R., Reylé, C., et al. 2021, *MNRAS*, 507, 2592, doi: [10.1093/mnras/stab2253](https://doi.org/10.1093/mnras/stab2253)
- Science Software Branch at STScI. 2012, *PyRAF: Python alternative for IRAF*, *Astrophysics Source Code Library*, record ascl:1207.011. <http://ascl.net/1207.011>
- Shajn, G. A., & Gaze, V. F. 1952, *Atlas of Diffuse Nebulae*
- Sharpless, S. 1953, *ApJ*, 118, 362, doi: [10.1086/145765](https://doi.org/10.1086/145765)
- Shull, J. M., & Kulkarni, S. R. 2023, *arXiv e-prints*, arXiv:2305.13449, doi: [10.48550/arXiv.2305.13449](https://doi.org/10.48550/arXiv.2305.13449)
- Slipher, V. M. 1913, *Lowell Observatory Bulletin*, 2, 56
- Smith, H. 2015, *MNRAS*, 449, 2980, doi: [10.1093/mnras/stv456](https://doi.org/10.1093/mnras/stv456)
- Smithsonian Astrophysical Observatory. 2000, *SAOImage DS9: A utility for displaying astronomical images in the X11 window environment*, *Astrophysics Source Code Library*, record ascl:0003.002. <http://ascl.net/0003.002>
- Sohn, S. T., Anderson, J., & van der Marel, R. P. 2012, *ApJ*, 753, 7, doi: [10.1088/0004-637X/753/1/7](https://doi.org/10.1088/0004-637X/753/1/7)
- Thilker, D. A., Braun, R., Walterbos, R. A. M., et al. 2004, *ApJL*, 601, L39, doi: [10.1086/381703](https://doi.org/10.1086/381703)
- Thilker, D. A., Braun, R., & Westmeier, T. 2005a, in *Astronomical Society of the Pacific Conference Series*, Vol. 331, *Extra-Planar Gas*, ed. R. Braun, 113
- Thilker, D. A., Hoopes, C. G., Bianchi, L., et al. 2005b, *ApJL*, 619, L67, doi: [10.1086/424816](https://doi.org/10.1086/424816)
- Trujillo, I., & Fliri, J. 2016, *ApJ*, 823, 123, doi: [10.3847/0004-637X/823/2/123](https://doi.org/10.3847/0004-637X/823/2/123)
- Tutone, A., Ballet, J., Acero, F., D'Ai, A., & Cusumano, G. 2021, *A&A*, 656, A139, doi: [10.1051/0004-6361/202141978](https://doi.org/10.1051/0004-6361/202141978)
- Tweedy, R. W., & Kwitter, K. B. 1996, *ApJS*, 107, 255, doi: [10.1086/192364](https://doi.org/10.1086/192364)
- van Buren, D., & McCray, R. 1988, *ApJL*, 329, L93, doi: [10.1086/185184](https://doi.org/10.1086/185184)
- van der Marel, R. P., Fardal, M., Besla, G., et al. 2012, *ApJ*, 753, 8, doi: [10.1088/0004-637X/753/1/8](https://doi.org/10.1088/0004-637X/753/1/8)
- van der Marel, R. P., & Guhathakurta, P. 2008, *ApJ*, 678, 187, doi: [10.1086/533430](https://doi.org/10.1086/533430)
- van Dokkum, P. G. 2001, *PASP*, 113, 1420, doi: [10.1086/323894](https://doi.org/10.1086/323894)
- Walterbos, R. A. M., & Kennicutt, R. C., J. 1987, *A&AS*, 69, 311
- Warmels, R. H. 1992, in *Astronomical Society of the Pacific Conference Series*, Vol. 25, *Astronomical Data Analysis Software and Systems I*, ed. D. M. Worrall, C. Biemesderfer, & J. Barnes, 115
- Weidmann, W. A., Ahumada, J. A., Gamon, R., et al. 2023, *NewA*, 98, 101932, doi: [10.1016/j.newast.2022.101932](https://doi.org/10.1016/j.newast.2022.101932)
- Weidmann, W. A., Schmidt, E. O., Vena Valdarenas, R. R., et al. 2016, *A&A*, 592, A103, doi: [10.1051/0004-6361/201527199](https://doi.org/10.1051/0004-6361/201527199)
- Werner, K., Reindl, N., Löbbling, L., et al. 2020, *A&A*, 642, A228, doi: [10.1051/0004-6361/202038574](https://doi.org/10.1051/0004-6361/202038574)
- West, J. L., Campbell, J. L., Bhaura, P., et al. 2022, *ApJ*, 941, 6, doi: [10.3847/1538-4357/ac9b58](https://doi.org/10.3847/1538-4357/ac9b58)
- Westmeier, T., Brüns, C., & Kerp, J. 2008, *MNRAS*, 390, 1691, doi: [10.1111/j.1365-2966.2008.13858.x](https://doi.org/10.1111/j.1365-2966.2008.13858.x)
- Wolfe, S. A., Pisano, D. J., Lockman, F. J., McGaugh, S. S., & Shaya, E. J. 2013, *Nature*, 497, 224, doi: [10.1038/nature12082](https://doi.org/10.1038/nature12082)
- Ziegler, M., Rauch, T., Werner, K., Kruk, J. W., & Oliveira, C. M. 2009, *Ap&SS*, 320, 257, doi: [10.1007/s10509-008-9789-4](https://doi.org/10.1007/s10509-008-9789-4)